Groundwater flow, heat transport, and water table position within volcanic edifices: Implications for volcanic processes in the Cascade Range

Shaul Hurwitz
U.S. Geological Survey, Menlo Park, California, USA

Kenneth L. Kipp
U.S. Geological Survey, Denver, Colorado, USA

Steven E. Ingebritsen and Mark E. Reid
U.S. Geological Survey, Menlo Park, California, USA

Received 1 May 2003; revised 8 August 2003; accepted 27 August 2003; published 11 December 2003.

[1] The position of the water table within a volcanic edifice has significant implications for volcano hazards, geothermal energy, and epithermal mineralization. We have modified the HYDROTHERM numerical simulator to allow for a free-surface (water table) upper boundary condition and a wide range of recharge rates, heat input rates, and thermodynamic conditions representative of continental volcano-hydrothermal systems. An extensive set of simulations was performed on a hypothetical stratovolcano system with unconfined groundwater flow. Simulation results suggest that the permeability structure of the volcanic edifice and underlying material is the dominant control on water table elevation and the distribution of pressures, temperatures, and fluid phases at depth. When permeabilities are isotropic, water table elevation decreases with increasing heat flux and increases with increasing recharge, but when permeabilities are anisotropic, these effects can be much less pronounced. Several conditions facilitate the ascent of a hydrothermal plume into a volcanic edifice: a sufficient source of heat and magmatic volatiles at depth, strong buoyancy forces, and a relatively weak topography-driven flow system. Further, the plume must be connected to a deep heat source through a pathway with a time-averaged effective permeability $\geq 1 \times 10^{-16}$ m^2, which may be maintained by frequent seismicity. Topography-driven flow may be retarded by low permeability in the edifice and/or the lack of precipitation recharge; in the latter case, the water table may be relatively deep. Simulation results were compared with observations from the Quaternary stratovolcanoes along the Cascade Range of the western United States to infer hydrothermal processes within the edifices. Extensive ice caps on many Cascade Range stratovolcanoes may restrict recharge on the summits and uppermost flanks. Both the simulation results and limited observational data allow for the possibility that the water table beneath the stratovolcanoes is relatively deep. *INDEX TERMS:* 1829 Hydrology: Groundwater hydrology; 3210 Mathematical Geophysics: Modeling; 3230 Mathematical Geophysics: Numerical solutions; 8424 Volcanology: Hydrothermal systems (8135); 9350 Information Related to Geographic Region: North America; *KEYWORDS:* groundwater flow, volcanic edifice, Cascade Range, water table, numerical simulations, stratovolcano

Citation: Hurwitz, S., K. L. Kipp, S. E. Ingebritsen, and M. E. Reid, Groundwater flow, heat transport, and water table position within volcanic edifices: Implications for volcanic processes in the Cascade Range, *J. Geophys. Res.*, *108*(B12), 2557, doi:10.1029/2003JB002565, 2003.

1. Introduction

[2] Groundwater dynamics within a volcanic edifice play a dominant role in volcano hazards, geothermal energy, and epithermal mineralization. The potential for slope failure, lahar generation, and phreatic eruptions is strongly dependent on the position of the water table within the volcanic edifice. In the unsaturated zone above the water table, pressures in the liquid phase are negative (subatmospheric) and can act as a weakly cohesive force in unconsolidated shallow material. In fully saturated porous media, fluid pressures are positive, reducing effective stress and increasing the potential for slope failure [*Terzaghi*, 1943; *Iverson*

This paper is not subject to U.S. copyright.
Published in 2003 by the American Geophysical Union.

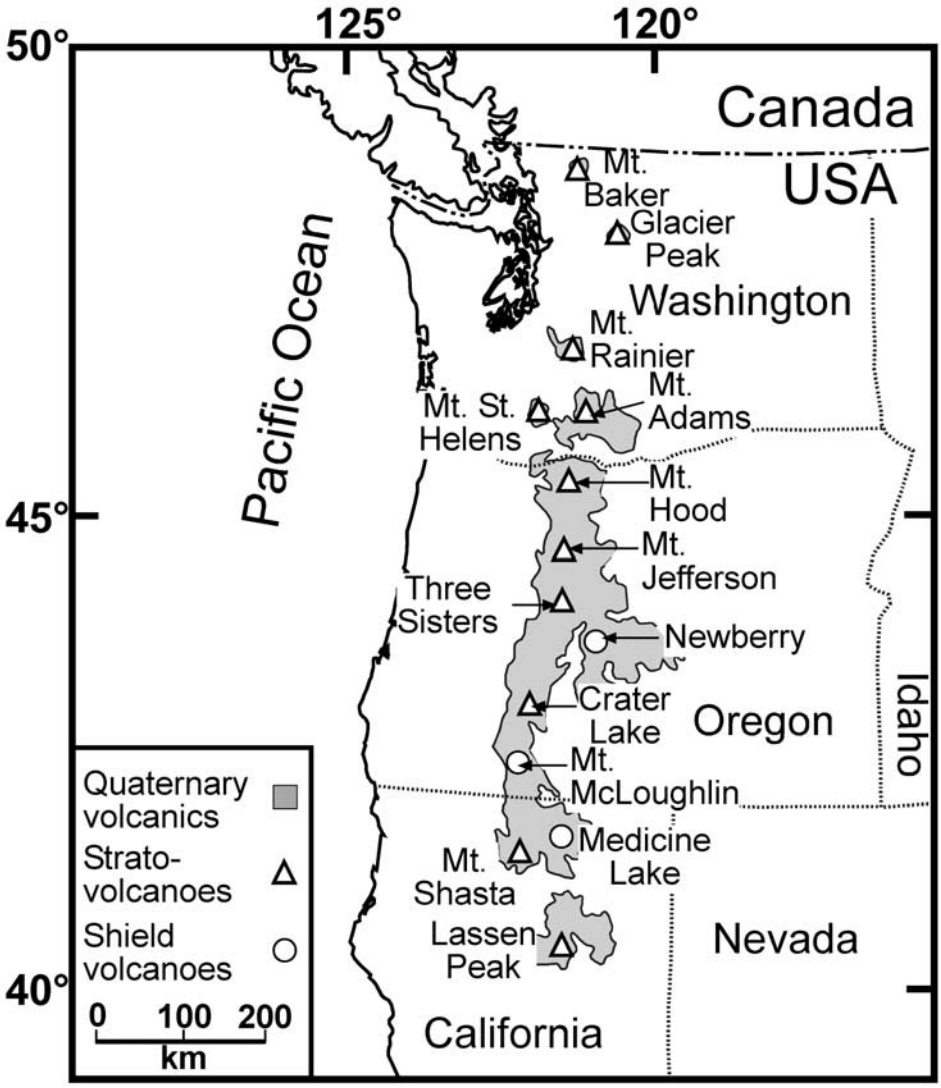

Figure 1. Map showing location of major volcanoes along the Cascade Range volcanic arc, northwestern United States.

and Reid, 1992; *Reid and Iverson*, 1992; *Lopez and Williams*, 1993]. Further, the rates, patterns, and mechanisms of pressure transmission and transport of heat and mass will be distinctly different in the unsaturated zone above the water table and the underlying saturated zone, for instance, pressure increases originating at depth will not be readily transmitted above the water table nor will solutes with an affinity for the liquid phase.

[3] There is little direct knowledge of water table elevation and geometry in active volcanic cones because few deep drill holes are located on or near volcanic summits. A single deep well on the summit of Kilauea Volcano, Hawaii, reveals that the water table is approximately 490 m below the ground surface [*Keller et al.*, 1979; *Hurwitz et al.*, 2002]. In humid regions such as Kilauea (1–3 m per year of precipitation [*Takasaki*, 1993]), hydrogeologists would typically expect to encounter the water table much closer to the land surface; its great depth at Kilauea reflects the high permeability of unaltered to weakly altered lava flows relative to most Earth materials. In fact, the pioneering hydrogeologist O.E. Meinzer referred to the hydrology of Hawaiian volcanoes as "...freakish in every respect..." [*Stearns and Clark*, 1930] mainly because of phenomena related to the high near-surface permeabilities.

[4] Though many volcanoes host summit crater lakes [e.g., *Varekamp and Rowe*, 2000], it is often unclear whether the surface of these lakes represents the water table elevation or that of a "perched" water body underlain by an unsaturated zone containing liquid water at subatmospheric fluid pressures. At Newberry Volcano, Oregon, a 932-m-deep well was drilled near the crater lakes, yet there is still disagreement as to whether the water table coincides with lake level [*Sammel et al.*, 1988] or is much deeper [e.g., *Black*, 1983].

[5] Previous numerical modeling studies provide limited insight into the factors controlling water table position within volcanic edifices. Pioneering studies of hydrothermal circulation such as those by *Norton and Knight* [1977] and *Cathles* [1977] neglected topography entirely and assumed single-phase flow. Later work by *Hayba and Ingebritsen* [1997] included multiphase (steam-liquid) flow and gave

some consideration to topography but assumed that water table position was fixed in space and time.

[6] A pioneering work on water table elevation in mountainous terrain [*Jamieson and Freeze*, 1983] was followed by the most relevant theoretical work to date on the subject [*Forster and Smith*, 1988a, 1988b, 1989]. These authors developed a finite element code allowing for a free-surface upper boundary condition and did a parametric analysis of the effects of topography, permeability, recharge, and heat flow on the elevation and geometry of the water table. Their study was limited to single-phase (liquid water) flow and invoked maximum heat flow values ($\leq$120 mW m^{-2}) that are considerably lower than those representative of most active volcanoes. *Forster and Smith* [1988b, 1989] also did not address the anisotropy of permeability (k_x generally $>k_z$), a factor that is often significant in volcanic terrains due to the layering of lavas [cf. *Souza and Voss*, 1987] and other flow deposits [cf. *Winograd*, 1971].

[7] In this paper we describe the results of numerical simulations of multiphase groundwater flow under conditions representing active volcanic systems with steep flanks. The simulations are conditioned on recharge rates (up to 1 m yr^{-1}), and heat input rates (10 s of megawatts or up to $\sim$4 W m^{-2}) typical of stratovolcanoes in the Cascade Range, northwest United States (Figure 1). Both the basic equations of groundwater flow and heat transport and the results of *Forster and Smith* [1988b, 1989] suggest that permeability structure, recharge rate, and heat input rate will be dominant controlling factors. The objective of these simulations is to quantify the relative importance of these factors in controlling water table elevation, phase distribution, and thermal structure within volcanic edifices. To account for relevant boundary conditions we have modified the high-temperature, multiphase groundwater flow and heat transport simulator HYDROTHERM [*Hayba and Ingebritsen*, 1994] by introducing a free-surface upper boundary condition.

[8] After summarizing the simulation results we attempt to relate them to the sparse field observations from volcanoes along the Cascade Range. We hope that this analysis will enhance understanding of flow and transport within volcanic edifices and help to guide additional fieldwork. Such an understanding has implications for geothermal and epithermal mineral resources as well as volcanic hazards.

2. Mathematical Approaches and Numerical Techniques

[9] The computer program HYDROTHERM [*Hayba and Ingebritsen*, 1994] simulates heat transport and two-phase (liquid and vapor) groundwater flow in three dimensions and includes pure water equations of state in the temperature range of 0°–1200°C and pressure range of 5×10^4–1×10^9 Pa. Finite difference numerical techniques are used for spatial and temporal discretization of the differential equations. Simultaneous solutions are obtained for the dependent variables, pressure and enthalpy, which together uniquely define the thermodynamic state of the system.

[10] We introduced several major modifications to the original HYDROTHERM code to enable our simulations. They include (1) the ability to simulate unsaturated groundwater flow, (2) precipitation recharge and seepage surface boundary conditions at the land surface, and (3) the ability to simulate variable temperature at a specified pressure boundary. This enhanced version of the code can simulate large-scale drainage of a saturated domain but is frequently unstable when simulating saturation of a zone containing stagnant air.

Table 1. Definition of Symbols in Equations

	Definition	Units
	Symbol	
$\hat{e}_z$	unit vector in the z-coordinate direction	(–)
g	gravitational constant	(m/s^2)
h	specific enthalpy	(J/kg)
$\mathbf{I}$	identity matrix of rank 3	(–)
$\bar{k}$	permeability tensor	(m^2)
k_r	relative permeability	(–)
K_m	medium thermal conductivity	(W/m-K)
Nu	Nusselt number	(–)
p	fluid pressure	(Pa)
p_c	capillary pressure	(Pa)
q	boundary flux or source/sink	(kg/m^2-s); (kg/m^3-s)
S	volumetric saturation	(–)
t	time	(s)
T	temperature	(°C)
∇T	temperature gradient	(°C/m)
$\mathbf{v}$	volumetric flux (Darcy velocity)	(m/s)
μ	viscosity	(Pa-s)
ρ	density	(kg/m^3)
ϕ	porosity	(–)
	Subscripts	
a	air	
c	capillary effects	
f	the flowing fluid mixture (single- or two-phase)	
g	gas	
H	enthalpy	
i	phase i	
m	the porous medium and fluid and gas	
R	precipitation recharge	
r	rock or residual saturation	
s	steam	
w	liquid water	

2.1. Flow and Transport Equations

[11] The groundwater flow equation is based on conservation of water mass in a volume element given by

$$\frac{\partial[\phi(\rho_w S_w + \rho_s S_s)]}{\partial t} - \nabla \frac{\bar{k} k_{rw} \rho_w}{\mu_w}[\nabla p + \rho_w g \hat{e}_z] - \nabla \frac{\bar{k} k_{rs} \rho_s}{\mu_s}[\nabla p + \rho_s g \hat{e}_z] - q_w - q_s = 0, \quad (1)$$

where p is pressure and the subscripts w and s refer to liquid water and steam, respectively; other symbols are defined in Table 1. The terms involving steam are not present in the air-water zone above the water table.

[12] Because any point in the simulation domain may be in either a single-phase zone, a two-phase one-component (steam-liquid water) zone below the water table, or a two-phase two-component (air-liquid water) zone above the water table, the saturation constraint equation is generalized to

$$S_w + S_g = 1, \quad (2)$$

where S_g represents the saturation of either steam or air. The volumetric flux or Darcy velocity for phase i is obtained from Darcy's Law as

$$\mathbf{v}_i = -\frac{\bar{k}k_{\mathrm{ri}}}{\mu_i}[\nabla p + \rho_i g \hat{e}_z]. \tag{3}$$

[13] The heat transport equation is based upon the conservation of enthalpy, a derived property containing both internal energy and flow energy, in both fluid and solid phases:

$$\frac{\partial}{\partial t}[\phi(\rho_w h_w S_w + \rho_s h_s S_s) + (1-\phi)\rho_r h_r] - \nabla \cdot K_m \nabla T + \nabla \cdot \phi \rho_w h_w \mathbf{v}_w + \nabla \cdot \phi \rho_s h_s \mathbf{v}_s - q_h = 0, \tag{4}$$

where K_m is an effective thermal conduction coefficient that does not depend on liquid saturation or porosity. A detailed derivation of the equation is given by *Faust and Mercer* [1979]. As was the case for the flow equation (1), the terms involving steam are not present in the air-water zone above the water table.

2.2. Water Table Position and Unconfined Flow

[14] The water table is defined as a surface of atmospheric pressure. From the fluid pressure field solution of HYDROTHERM we calculate the position of a water table in each column of the simulation domain. Capillary pressure, which is the pressure difference between the liquid and gas phases in the two-phase (air-water) zone above the water table, is defined by

$$p_c = p_a - p_w. \tag{5}$$

Linear functions were adopted for water saturation and for relative permeability as a function of capillary pressure. The linear water saturation function is

$$\frac{1-S_w}{1-S_{\mathrm{wr}}} = \frac{p_c - p_{\mathrm{cb}}}{p_{\mathrm{cr}} - p_{\mathrm{cb}}} \qquad \text{for} \quad p_{\mathrm{cb}} < p_c < p_{\mathrm{cr}}, \tag{6a}$$

$$S_w = 1 \qquad \text{for} \quad p_c \le p_{\mathrm{cb}}, \tag{6b}$$

$$S_w = S_{\mathrm{wr}} \qquad \text{for} \quad p_c \ge p_{\mathrm{cr}}, \tag{6c}$$

where p_{cb} is the capillary pressure at the bubbling point and p_{cr} is the capillary pressure at the residual water saturation. Liquid flow ceases for $p_c \ge p_{\mathrm{cr}}$. In dry environments or in areas with deep water tables, the capillary pressure can be very large and the corresponding liquid-phase pressure can be a large negative value. The HYDROTHERM equation-of-state tables are limited to pressures greater than 5×10^4 Pa (0.5 atm), and we arbitrarily enforce this lower limit for water property calculations in the air-water zone. This approximation is unlikely to induce any serious error to the simulations because at low hydrodynamic pressures there is little heat transport by advection.

2.3. Recharge Boundary Condition

[15] For unconfined groundwater systems a useful land surface boundary condition is a precipitation recharge flux with associated heat advection. This can be treated as a net flux after accounting for evapotranspiration. Heat advection q_{HR} at such a boundary S_R is given by

$$q_{\mathrm{HR}}(\mathbf{x}) = h_R(T,p)\rho_R(T,p)q_{\mathrm{FR}} \qquad \text{for} \quad \mathbf{x} \quad \text{on} \quad S_R, \tag{7}$$

where the precipitation enthalpy h_R and density ρ_R are calculated at a specified temperature and atmospheric pressure, q_{FR} is the recharge flux across the land surface boundary ($\mathrm{m}^3\ \mathrm{m}^{-2}\ \mathrm{s}^{-1}$), S_R is the area over which the precipitation boundary condition exists (m^2), and $\mathbf{x}$ is the vector of spatial position along boundary S_R. The recharge flux flows generally downward through the partially saturated zone to the water table.

2.4. Surface-of-Seepage Boundary Condition

[16] A surface-of-seepage boundary condition allows groundwater discharge to occur where the water table intercepts a sloping land surface. We implement this condition along sloping boundaries by using alternating thin (z dimension $\gg r$ dimension) "seeping" cells and wide ($z \ll r$) cells (Figure 2, inset). The seeping cells allow horizontal discharge, and the wide cells allow vertical precipitation recharge at a specified rate.

[17] Along a sloping land surface, such as a mountainside or volcanic cone, a seepage surface often occupies the lower portion of the slope, whereas the upper portion receives precipitation recharge. The "hinge point" for steady state flow between seepage and recharge can be adjusted iteratively [e.g., *Forster and Smith*, 1988a]. Our discretization approach obviates the need to iteratively relocate the hinge point: a seeping cell becomes nonseeping if the seepage rate becomes positive (inflow to the domain); conversely, nonseeping cells become seeping cells if pressure rises above atmospheric pressure. These tests are applied at the end of each time step in the numerical scheme. If any seeping cell switches condition, the subsequent time step reflects the new boundary condition state.

2.5. Modified Constant Pressure-Enthalpy Boundary Condition

[18] In multidimensional simulations of groundwater flow and heat transport, the upper (land surface) boundary is commonly treated as a constant pressure and constant enthalpy (or temperature) boundary. Constant-in-time lateral boundaries also are common. The version of HYDROTHERM documented by *Hayba and Ingebritsen* [1994], like most hydrothermal models, requires that both pressure and enthalpy be held constant-in-time at a boundary for each simulation period. In the modified version of the simulator, these conditions were decoupled, allowing for advective flux of enthalpy through a boundary with constant pressure. For flow into the domain, the enthalpy (or temperature) of the incoming fluid is specified, and for outflow, the enthalpy of the outgoing fluid is that of the ambient fluid at the boundary and is determined by solution of the heat transport equation. This combination of flow and heat transport boundary conditions will be referred to as specified pressure and associated enthalpy (temperature)

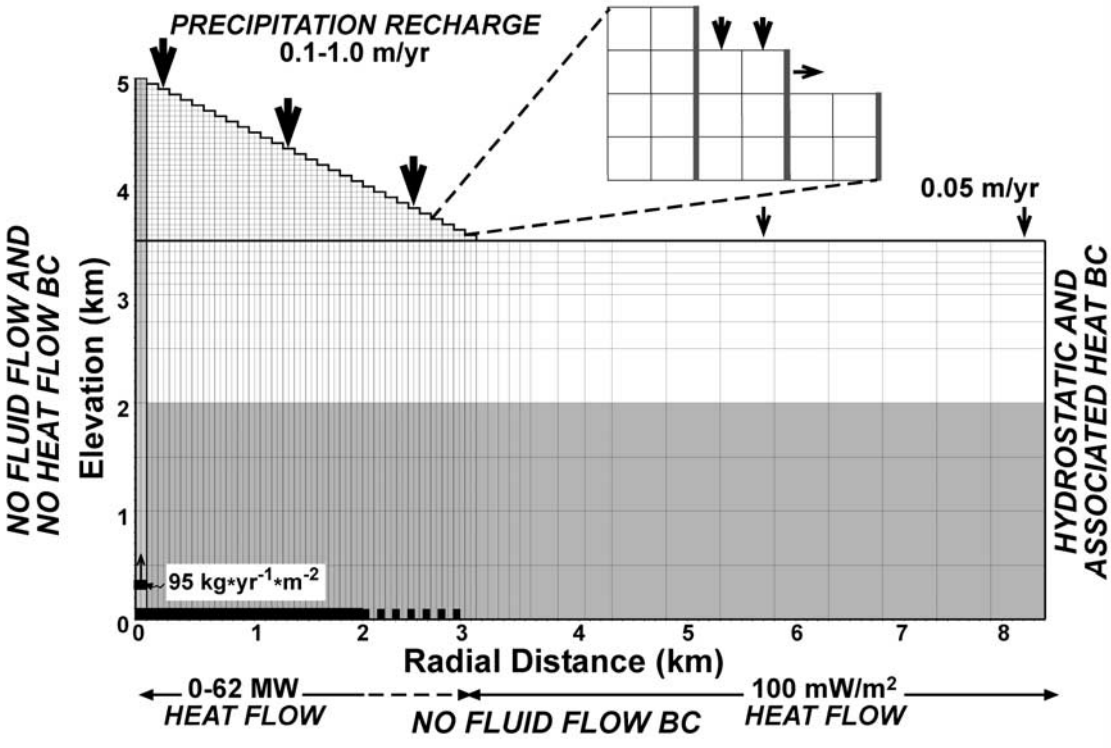

Figure 2. Finite difference grid employed in numerical simulations. Shading indicates low-permeability basal unit. Also shown are the area with high basal heat flow (thick line on bottom left); a high-vertical-permeability conduit adjacent to the left-hand boundary incorporated in simulation series J, K, and L; and location of the mass source incorporated in simulation series L. Inset shows recharge and seepage boundary cells on the cone. See Table 3 for descriptions of simulation series.

boundary conditions. Under certain flow regimes this approach leads to more realistic estimates of near-boundary temperatures.

3. Simulation Assumptions and Simplifications

[19] The most important simplification in our numerical simulation study is the emphasis on quasi steady state solutions obtained for particular sets of boundary conditions and parameter values. This approach is similar to previous studies that solved equations for steady state groundwater flow and heat transport [*Forster and Smith*, 1988a, 1988b, 1989]. We emphasize steady state results because this allows us to more readily isolate the sensitivity of key parameters and boundary conditions. However, natural volcanic hydrothermal systems likely never achieve a true steady state. To obtain quasi steady state solutions we ran transient simulations to near equilibrium; this entailed simulation times of 30,000–50,000 years. This timescale for near equilibrium is long compared to the eruption intervals of active Cascade Range volcanoes, which are on the order of 200–2000 years. Further, in some rapidly deforming or highly reactive systems, the key controlling parameter, permeability, can vary on timescales of less than 1 year [*Nur and Walder*, 1992; *Martin and Lowell*, 1997; *Moore et al.*, 1994; *Hurwitz et al.*, 2002].

[20] Several other simplifying assumptions are not significantly limiting for purposes of this study. For example, the circulating fluid was assumed to be pure water, and the finite difference approach used by HYDROTHERM requires us to represent the edifice by stairsteps rather than a plane slope (Figure 2). In the lack of much experimental and theoretical data for volcanic rocks at high temperature, we selected a linear relative permeability function between liquid and steam zones. Additional assumptions specific to the work reported here are (1) a simplified linear saturation curve and relative permeability function between the land surface and the water table, (2) an artificially high value for capillary pressure at residual water saturation in order to facilitate precipitation recharge and the approach to steady state, and (3) no water vapor in the gas (air) phase, meaning that boiling at the water table cannot be simulated. These simplifications are consistent with our emphasis on steady state results and our lack of interest in the exact dynamics of flow in the unsaturated zone above the water table. We also ignored any thermal lapse rate in the precipitation recharge (likely 5°–6°C per km elevation); instead, we invoked a constant value of 5°C. Similarly, we neglected variation of atmospheric pressure with elevation. *Hayba and Ingebritsen* [1994] list and discuss assumptions incorporated into the previous version of HYDROTHERM.

4. Model Configuration and Boundary and Initial Conditions

[21] The model domain is a radial cross section through a cylinder of radius 8.3 km and height 3.5 km overlain by a cone with base radius 3.0 km and height 1.5 km (Figure 2).

Table 2. Constant Simulation Parameters

Parameter	Value
Porosity of basal unit	0.01
Porosity of conduit	0.15
Thermal conductivity of basal unit	2.5 W m^{-1} K^{-1}
Thermal conductivity of upper unit	2.0 W m^{-1} K^{-1}
Thermal conductivity of conduit	2.0 W m^{-1} K^{-1}
Rock density	2500 kg m^{-3}
Precipitation temperature	5°C
Radius of intense heat source	2.1 or 2.9 km
Radius of cylindrical region	8.3 km
Precipitation on the cylinder upper boundary	0.05 m yr^{-1}
Background basal heat flow	100 mW m^{-2}

The left edge of the cross section coincides with the central axis of the cylinder and cone. The cone, representing the edifice, has a surface slope of 27°. The cross section is divided into 105 columns and 43 rows, with 2760 active cells. Simulations were carried out using cylindrical coordinates and representative boundary conditions.

[22] The left-hand boundary was treated as insulating and impermeable. The upper (land surface) boundary was divided into two regions. The horizontal region of the upper boundary was assigned a net precipitation flux of 0.05 m yr^{-1} in all simulations (Table 2), whereas the net precipitation flux on the cone region was specified for each simulation (Table 3). The temperature of the net precipitation flux in both regions was 5°C. The right-hand boundary was maintained at the initial hydrostatic fluid pressure and the associated fluid temperature. The bottom boundary was impermeable and was divided into two zones, each with a specified constant heat flux: a zone with a radius of either 2100 or 2950 m beneath the cone with very high heat flux of up to 2700 mW m^{-2} (up to 62 MW total heat input) representing a magmatic heat source and a zone at larger radial distances with a basal heat flux of 100 mW m^{-2} representing typical geothermal conditions in Quaternary volcanic terrain [*Hasabe et al.*, 1970; *Ingebritsen et al.*, 1994].

[23] Initial pressure conditions were 1 atm between elevations of 3500 m (base of cone) and 5000 m (peak) and a hydrostatic pressure distribution between 3500 m and the base of the domain. These initial conditions result in a fully saturated flow system ($S_w = 1$ at $t = 0$). Initial temperatures were based on a temperature of 5°C at the ground surface and a thermal gradient of 50°C km^{-1}.

5. Key Parameters

[24] In this section we discuss the open questions and the hypotheses that motivate the parameters selected for examination, and the plausible ranges for the simulation parameters listed in Tables 2 and 3. The hydrodynamic regime in an active volcano will depend primarily on the magmatic heat supply, the pattern and rates of precipitation (and other) recharge, and the permeability structure of the edifice. The latter is subject to the greatest uncertainty. In crystalline rock, permeabilities are highly heterogeneous and range over at least eight orders of magnitude at the scale of in situ hydraulic testing [*Brace*, 1980, 1984]. This huge range results largely from the variability of fracture density, aperture, and geometry and is also strongly influenced by the degree of hydrothermal alteration and fracture filling. Further, volcanic cones consist mainly of roughly slope-parallel layered lava flows and pyroclastic units. This implies that permeability anisotropy should be significant, at least at shallow depths. Direct measurements of permeability anisotropy are rare, and it is often neglected in numerical models. In some simulations, we examined the general effects of anisotropic permeability by varying the ratio of horizontal (k_x) to vertical (k_z) permeability.

[25] Previous numerical simulations of groundwater flow and heat transport in the Cascade Range [*Ingebritsen et al.*, 1992] invoked permeabilities on the order of 10^{-14} m^2 for Quaternary volcanic rocks in order to simulate the nearly isothermal temperature profiles observed at relatively shallow depths. Lower permeabilities on the order of 10^{-16} m^2 or less were required to successfully simulate the conduction-dominated thermal regime observed in older rocks at greater depths [*Sammel et al.*, 1988; *Ingebritsen et al.*, 1992].

[26] The near-surface permeabilities required to accommodate the high precipitation recharge rates observed in Quaternary rocks of the Oregon Cascade (0.7–1.3 m yr^{-1} [*Ingebritsen et al.*, 1992; *Manga*, 1997]) are on the order of 10 [*Ingebritsen et al.*, 1992] to 10^3 times [*Manga*, 1996] larger than those that provide best matching of the near-surface thermal regime. To effectively match both the recharge rate and the thermal observations requires a strong decay in permeability between the land surface and ~1-km depth. Therefore in a few simulations presented here (series K), we invoked a stepwise permeability decrease with depth that approximates the permeability-depth curve for the active continental crust suggested by *Manning and Ingebritsen* [1999]. In these simulations, permeability was 1×10^{-13} m^2 (isotropic) in the upper 1 km and decreased stepwise to 1×10^{-17} m^2 at the base of the model, and recharge on the cone was 1.0 m yr^{-1}. To represent the possible influence of a high-vertical-permeability conduit for ascending magmatic fluids we included a permeable conduit adjacent to the left-hand boundary (Figure 2) in a few simulations (series J and L). However, in most simulations reported here we did not attempt to represent complexities such as depth-dependent permeability or vertical structures but instead invoked a simple two-layer permeability model similar to that employed by *Forster and Smith* [1988a, 1988b, 1989] (Figure 2).

[27] Advective heat discharge from Cascade Range hydrothermal features can be used as a crude proxy for magmatic heat input because both geochemical data and thermal arguments indicate that many hot spring groups represent lateral outflow from Quaternary silicic volcanic centers [*Ingebritsen et al.*, 1989]. Heat transfer rates for individual Cascade Range hot spring groups vary from <1 to ~90 MW [*Mariner et al.*, 1990; *Ingebritsen et al.*, 1994]. A heat loss of 1 MW translates to crystallization and cooling of silicic magma at a rate of 15–20 km^3 Ma^{-1} [*Ingebritsen and Sanford*, 1998, p. 183]. Thus the larger hot spring heat transfer rates observed in the Cascade Range are unlikely to be sustained over geologic time though they have been shown to be essentially constant over a multidecadal timescale [*Ingebritsen et al.*, 2001]. Estimates of heat discharge rates from summit fumaroles are relatively rare and range from ~10 MW at Mt. Hood [*Friedman et al.*, 1982] and Mt. Rainier [*Frank*, 1995] to 12–82 MW at Mt. Baker in

Table 3. Parameters and Water Table Elevations for Selected Simulations

Run	Upper $-\log k_x$, m^2	Upper $-\log k_z$, m^2	Basal $-\log k$, m^2	Conduit $-\log k$, m^2	Upper Porosity (−)	Heat Input, MW	Basal Thickness, m	Recharge Rate, m yr^{-1}	Water Table Elevation,[a] m
Series A: Varying Isotropic Permeability									
A1	14	14	17	...	0.1	14	2000	0.1	3578
A2	14.3	14.3	17	...	0.1	14	2000	0.1	3676
A3	15	15	17	...	0.1	14	2000	0.1	4258
A4	15.4	15.4	17	...	0.1	14	2000	0.1	4988
A5	13.5	13.5	17	...	0.1	14	2000	0.1	3538
Series B: Varying Anisotropic Permeability									
B1	12	15	17	...	0.1	14	2000	0.1	3513
B2	13	15	17	...	0.1	14	2000	0.1	3558
B3	14	15	17	...	0.1	14	2000	0.1	3720
Series C: Varying Heat Input, Isotropic Permeability									
C1	15	15	17	...	0.1	0	2000	0.1	4285
C2	15	15	17	...	0.1	28	2000	0.1	4224
C3	15	15	17	...	0.1	38	2000	0.1	4200
C4	15	15	17	...	0.1	62[b]	2000	0.1	4159
Series D: Varying Heat Input, Anisotropic Permeability									
D1	14	15	17	...	0.1	0	2000	0.1	3727
D2	14	15	17	...	0.1	28	2000	0.1	3710
D3	13	15	17	...	0.1	0	2000	0.1	3561
D4	13	15	17	...	0.1	28	2000	0.1	3550
Series E: Varying Recharge, Isotropic Permeability									
E1	15	15	17	...	0.1	14	2000	0.2	4845
E2	15	15	17	...	0.1	14	2000	0.3	5000
E7	14	14	17	...	0.1	14	2000	1	4313
E8	13	13	17	...	0.1	14	2000	1	3584
E13	13	13	17	...	0.1	14	2000	0.5	3534
Series F: Varying Recharge, Anisotropic Permeability									
F1	14	15	17	...	0.1	14	2000	0.2	4073
F2	14	15	17	...	0.1	14	2000	0.3	4935
F3	13	15	17	...	0.1	14	2000	0.2	3673
F4	13	15	17	...	0.1	14	2000	0.3	4880
Series G: Varying Thickness of Basal Unit									
G1	15	15	17	...	0.1	14	1500	0.1	4244
G2	15	15	17	...	0.1	14	2500	0.1	4282
Series H: Varying Permeability of Basal Unit									
H1	15	15	16	...	0.1	14	2000	0.1	4180
H2	15	15	19	...	0.1	14	2000	0.1	4259
Series I: Varying Porosity									
I1	15	15	17	...	0.01	28	2000	0.1	4258
I2	15	15	17	...	0.25	28	2000	0.1	4256
Series J: With a Permeable Vertical Conduit									
J1	15	15	16	12	0.1	35	2000	0.1	3712
J2	15	15	16	13	0.1	35	2000	0.1	3818
Series K: Stepwise Permeability Decrease With Depth									
K1	...	...		...		62[b]	...	1	3909
K2	...	...		13		54[b]	...	1	3907
Series L: "Magmatic" (550°C) Fluid Flux of 95 kg $yr^{-1}m^{-2}$ at r = 0–100 m									
L1	15	15	17	14.3	0.1	14	2000	0.1	4244
L2	15	15	16	12	0.1	14	2000	0.1	3921
L3	15	15	16	...	0.1	14	2000	0.1	4167
L4	15	15	17	...	0.1	14	2000	0.1	4257
L5	14	15	16	...	0.1	14	2000	0.1	3690

[a]Elevation in the column on the left-hand side of the domain (under summit of cone).
[b]Radius of high heat flow source is 2940 m.

1975 [*Frank and Post*, 1976] (see Figure 1 for locations of Cascade Range volcanoes). Apart from the clear transient increase observed at Mt. Baker in 1975, there are few data on the time variation of heat discharge from summit fumaroles. We assumed magmatic heat input rates of 0–62 MW in the different simulations (Table 3).

[28] Few models of volcano-hydrothermal systems have examined the role of a magmatic fluid as a mass source. *Hanson* [1996] showed that several factors act to focus magmatic fluids within young transient hydrothermal systems so that magmatic fluids can locally dominate meteoric fluids. The upward flux of magmatic fluids depends mainly on the depth, composition, and dimensions of the magma body. In selected simulations we included a mass source at the bottom-left corner of the domain (radius 0–100 m) to represent magmatic fluid input (series L). The flux that we invoked (95 kg yr^{-1} m^{-2} at 550°C) is within the range simulated by *Hanson* [1996].

[29] Parameters other than permeability, recharge rate, and heat input rate (Table 3) display much less variability and are secondary. The upper simulation unit, consisting of the cone and the upper part of the cylinder (Figure 2), was assigned a constant thermal conductivity of 2.0 W m^{-1} K^{-1}, consistent with the range of thermal conductivities measured on core and cuttings from the Cascade Range [*Blackwell et al.*, 1982; *Ingebritsen et al.*, 1994]. A slightly larger thermal conductivity of 2.5 W m^{-1} K^{-1} was assigned to the basal unit because at temperatures higher than about 500°C, radiation becomes an important heat transfer mechanism, resulting in higher thermal conductivities [*Clauser*, 1988; *Buettner et al.*, 1998].

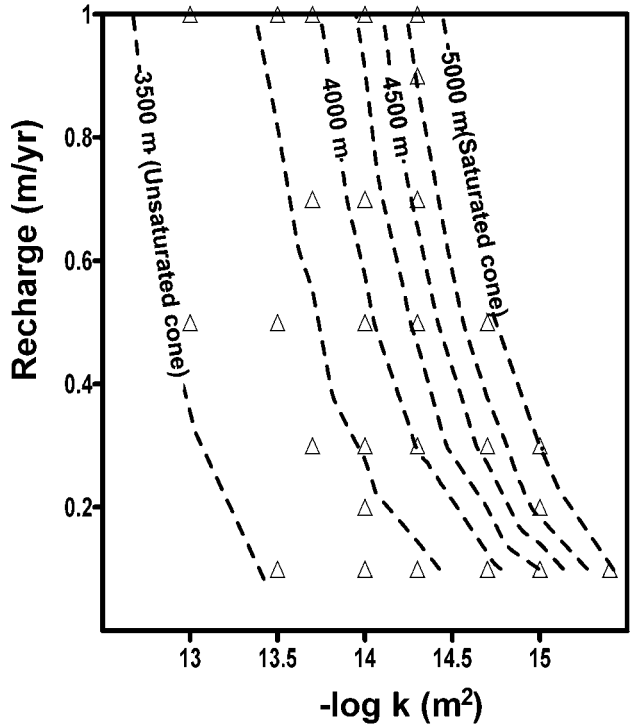

Figure 3. Elevation of the water table under the peak of the volcano as a function of isotropic permeability and precipitation recharge. Heat input in these simulations was 14 MW and the permeability of the 2-km-thick basal unit (Figure 2) was 1×10^{-17} m^2. Triangles represent simulation results.

6. Results

[30] Results from a suite of numerical experiments are summarized in Table 3 and Figures 3–13. These show steady state water table elevations, isotherms, fluid-phase distributions, groundwater flow vectors, and temperature and pressure profiles for selected simulations. The simulations were run in a transient mode (equations (1)–(4)) to quasi steady state (30,000–50,000 years); the criteria for determining an approximate steady state were a global heat and mass balance (output and input agreeing to within 1%) and a stable water table configuration (sum of absolute changes for all columns between successive 200-year-long time steps less than 10 m).

[31] In most cases we treated the upper simulation unit, which includes the cone and the upper 1500 m of the cylinder (Figure 2), as homogeneous and either isotropic or anisotropic with respect to permeability. The range of isotropic permeabilities that we were able to consider was effectively limited by the amount of recharge that could be accepted (at low k values) and the penetration of cold recharge to great depths at high k values (Figure 3). For vertical permeabilities (k_z) $<5 \times 10^{-15}$ m^2, recharge rates $\geq$0.1 m yr^{-1} cause ponding on the upper boundary of the domain. For vertical permeabilities $>1 \times 10^{-13}$ m^2, cold precipitation recharge flows rapidly to great depths (<10°C water at depths exceeding 2 km) such that the enthalpy at ambient pressure is outside the HYDROTHERM equation-of-state tables. Precipitation recharge of 1 m yr^{-1} requires $k \geq 1 \times 10^{-14}$ m^2 in the upper unit. With a heterogeneous permeability structure in the domain, high near-surface k_z (1×10^{-13} m^2), and a strong depth-dependence of k_z (Table 3, simulation series K1), we were able to simulate recharge rates of 1.0 m yr^{-1} and a large basal heat input (62 MW). Varying porosity has no effect on the steady state results (series I in Table 3).

[32] Relatively small changes in the values of the key controlling parameters, particularly permeability and its anisotropy, can lead to very large changes in water table elevation, thermal structure, and phase distribution. Water table position is sensitive to the value of isotropic permeability (Figure 4a and Table 3, simulation series A), consistent with the results of *Forster and Smith* [1988a, 1988b, 1989]. Low permeability and high recharge leads to a saturated edifice, whereas high permeability and low recharge lead to a deep water table. However, the elevation of the water table is less sensitive to the value of k_x for a fixed value of k_z (Figure 4b and Table 3, simulation series B).

[33] Variations in the basal heat input have a large effect on the deep thermal structure but little effect on water table elevation for both isotropic (Figure 5a and Table 3, simulation series C) and anisotropic permeabilities (Figure 5b and Table 3, simulation series D). In contrast, variations in the precipitation recharge rate have a large effect on water table elevation (Figure 3) and a minor effect on the deep thermal structure for both isotropic (Figure 6a) and anisotropic (Figure 6b) permeabilities (Table 3, simulation series E and F, respectively).

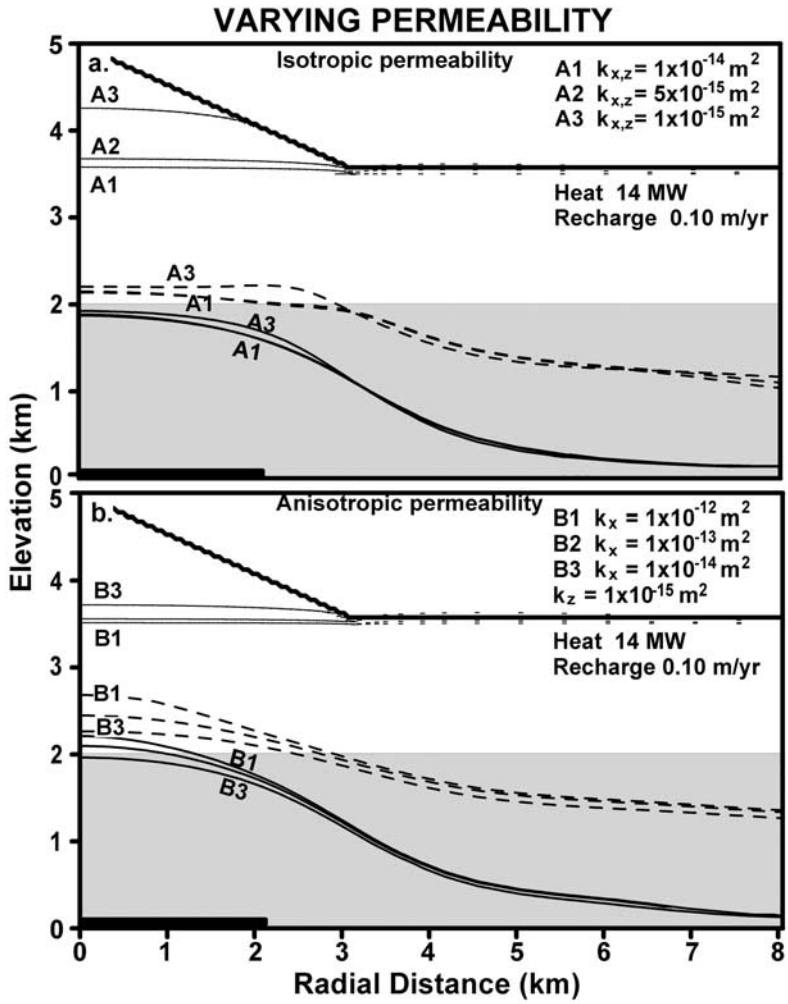

Figure 4. Effects of (a) varying isotropic permeability, with constant heat input and recharge rates (Table 3, simulation series A) and (b) varying anisotropic permeability, with constant heat input and recharge rates (Table 3, simulation series B). Thin lines indicate water table elevations; thick dashed and solid lines indicate 100° and 150°C isotherms, respectively. Gray shading is basal unit. See Table 3 for details of individual simulations.

[34] The simulation results are not particularly sensitive to the thickness of the low-permeability basal unit (Figure 7a and Table 3, simulation series G), but its permeability (Table 3, simulation series H) has a large effect on the thermal structure (Figure 7b), hydrodynamics, and distribution of fluid phases. Under steady state conditions, the intense basal heating at the center of the simulation domain generates a convective flow pattern at depth. In all simulations with a basal heat input $\geq$14 MW, supercritical fluid and steam occur in the basal unit (Figure 8). For basal unit permeabilities $\leq 1 \times 10^{-17}$ m^2, lower density fluids are confined to the basal unit. When basal unit permeability is increased to 1×10^{-16} m^2, advective heat transport at depth becomes significant and a steam plume can rise to near the water table (Figures 9c, 11c, and 11d). Cold recharge also penetrates the basal unit, and a much more active convection cell forms. The permeability threshold of about 1×10^{-16} m^2 for transition from conduction- to advection-dominated conditions, clearly evident in this result, is similar to that defined by previous studies [*Norton and Knight*, 1977; *Smith and Chapman*, 1983; *Manning et al.*, 1993; *Hayba and Ingebritsen*, 1997].

[35] In simulation series J (Table 3) we introduce a high-vertical-permeability conduit with a radius of 100 m at the center of the simulation domain (Figure 2). Beneath the center of the cone this enhances cold recharge, reduces temperatures, and suppresses steam formation. If basal unit permeability is $\geq 1 \times 10^{-16}$ m^2 a hydrothermal plume will still develop, but it is offset toward the flanks rather than centrally located (Figures 10a and 10b, compare simulations J1 and J2 with simulation H1 in Figure 9c).

[36] In simulation series K (Table 3) we invoke a stepwise approximation of *Manning and Ingebritsen*'s [1999] permeability-depth relation ($\log k = -14 - 3.2 \log z$, with z in kilometers). This permeability-depth relation, with near-surface $k = 1 \times 10^{-13}$ m^2 and $k = 1 \times 10^{-17}$ m^2 at the base of the cylinder, permits both high precipitation recharge rates (1 m yr^{-1}) and high basal heat input rates (62 MW). The active topography-driven flow system confines steam to the deep sections of the domain (Figure 10c:

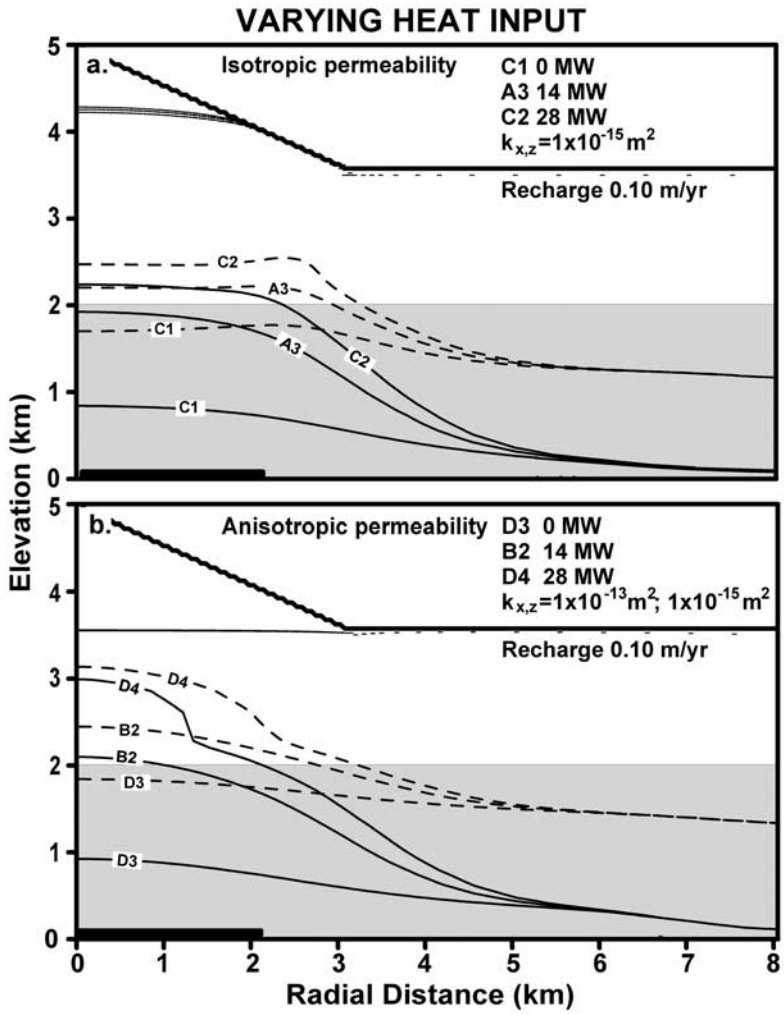

Figure 5. Effects of varying heat input with (a) isotropic permeability and recharge rate and (b) anisotropic permeability and recharge rate. Thin lines indicate water table elevations; thick dashed and solid lines indicate 100° and 150°C isotherms, respectively. Gray shading is basal unit. See Table 3 for details of individual simulations.

simulation K1). If a vertical conduit is added to this permeability structure, cold recharge is enhanced and isotherms beneath the summit are further suppressed (Figure 10d: simulation K2).

[37] In simulation series L we include a mass source at depth to represent the effects of fluid released by crystallizing magma. We invoke a flux of 95 kg yr^{-1} m^{-2} at 550°C over r from 0 to 100 m. This value is within the range simulated by *Hanson* [1996] and equates to about 0.1 kg s^{-1} of mass and 0.2 MW of heat. It is compatible with the focused heat input rate for this simulation series (14 MW) if one assumes that the heat is derived from cooling magma releasing ~0.5 wt % water. Such rates of fluid input at depth have a negligible effect on the elevation of the water table (Table 3: compare simulations A3 and H1, without a mass source at depth, to equivalent L4 and L3 with a mass source). However, the deep mass source has a significant effect on temperature and the distribution of fluid phases. In simulations L3 and L5 with a deep fluid source (Figure 11) a boiling plume extends all the way to the water table, whereas the top of the boiling plume falls several hundred meters short of the water table in a comparable simulation without a deep fluid source (Figure 9: simulation H1). In simulations with both a deep fluid source and a central, high-vertical-permeability conduit, cold recharge penetrates deep into the domain and suppresses temperatures (Figure 11: simulations L1 and L2).

[38] Simulated fluid pressures within and below the cone depend in large part on the water table elevation and the mixture of fluid phases present at depth. The range of possible pressures is roughly bracketed by cold water hydrostats with zero-pressure intercepts at 0- and 1500-m depth (Figure 12). In cases with moderate permeabilities and high recharge rates, there must be a large vertical gradient for downward flow such that the pressure gradient below the water table is significantly less than hydrostatic (Figure 12: simulation E2). The pressure gradient can also be subhydrostatic where low-density fluids (steam, supercritical fluid, boiling mixtures) are present at depth

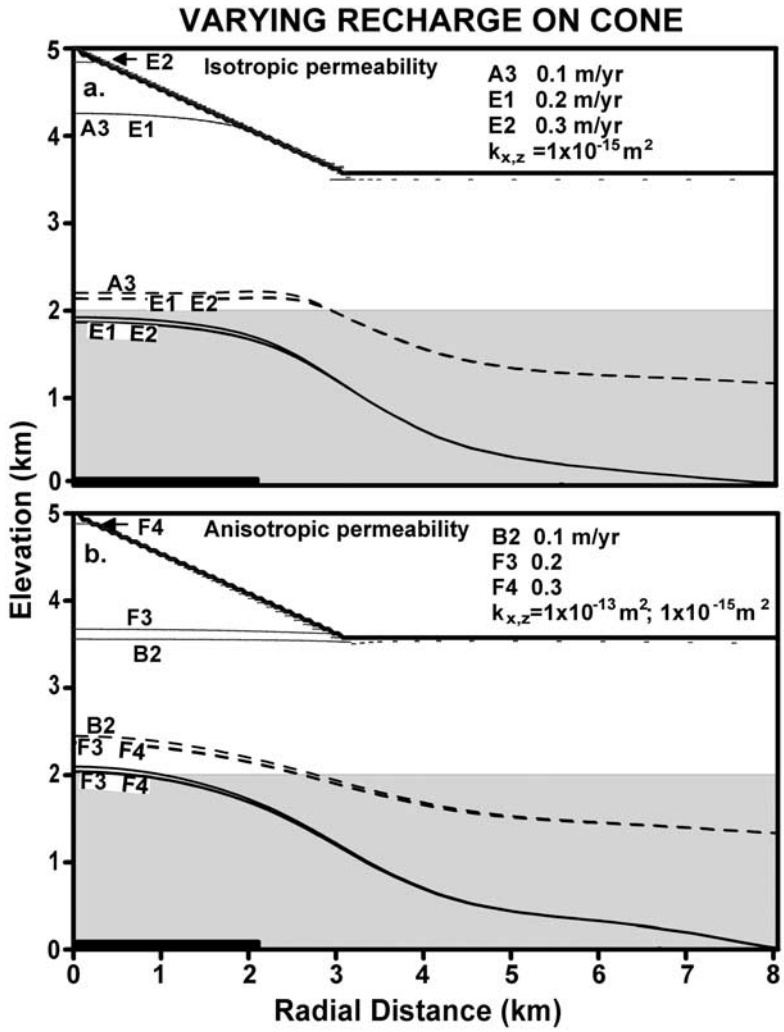

Figure 6. Effects of varying recharge rate on the cone with (a) isotropic permeability and heat input and (b) anisotropic permeability and heat input. Thin lines indicate water table elevations; thick dashed and solid lines indicate 100° and 150°C isotherms, respectively. Gray shading is basal unit. See Table 3 for details of individual simulations.

(Figure 12, departures from hydrostatic gradient below ~3-km depth). The calculated pressure profile for simulation L3 (Figure 12) indicates that the mass flux that we invoked in simulation series L had little effect on fluid pressures at depth.

[39] In most simulations, heat transport is advection dominated in the upper unit and conduction dominated in the lower permeability basal unit. To evaluate the relative efficiency of advective and conductive heat transport within the simulation domain, we compute a cell Nusselt number, *Nu*, the ratio of advective plus conductive heat flux to conductive heat flux alone, using the magnitudes of the two vector components:

$$Nu = \frac{|\rho_f v_f| h_f + K_m |\nabla T|}{K_m |\nabla T|}. \quad (8)$$

[40] The vector components of the temperature gradient are computed using a three-point difference formula spanning the node location. The subscript *f* indicates properties of the flowing fluid mixture (single or two phase). The value of *Nu* approaches 100 in parts of the upper unit and is generally <2 in the lower unit when the permeability of that unit is $k \leq 1 \times 10^{-17}$ m^2 (Figure 13). The extremely high value of log *Nu* (4.6) at depth in simulation H1 (Figure 13) illustrates efficient transport of heat by advection adjacent to the left-hand boundary when the basal permeability is at least 1×10^{-16} m^2.

7. Discussion

[41] The modified version of the HYDROTHERM simulator used in this study allows improved representation of volcanic hydrothermal systems. It permits exploration of a free-surface (water table) upper boundary configuration and a wide range of recharge rates, heat input rates, and hydraulic parameters.

7.1. Permeability as a Controlling Parameter

[42] The permeability structure of the volcanic edifice and underlying material is the dominant control on many

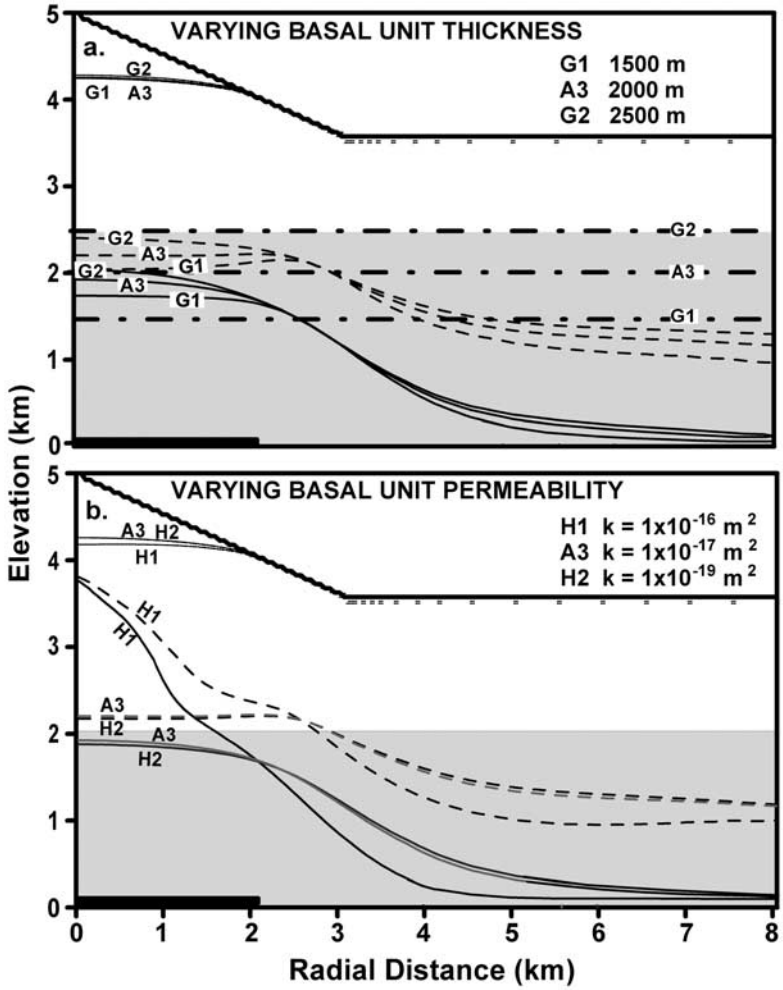

Figure 7. Effects of varying (a) basal unit thickness and (b) basal unit permeability. Thin lines indicate water table elevations; thick dashed and solid lines indicate 100° and 150°C contours, respectively. Gray shading is basal unit. See Table 3 for details of individual simulations.

system state variables of interest, including water table configuration and, more generally, the distribution of pressures, temperatures, and fluid phases at depth. For a given permeability structure, variations in heat input have a small effect on water table elevation and a large effect on the deep thermal structure (Figures 4a and 4b), whereas variations in the precipitation recharge rate have a large effect on water table elevation and a small effect on the deep thermal structure (Figures 5a and 5b).

[43] When permeabilities are isotropic, water table elevation decreases with increasing heat flux, consistent with results of *Forster and Smith* [1988b, 1989] (Figure 5a). This is because high heat flow tends to decrease fluid viscosity, increasing hydraulic conductivity so that the same amount of topography-driven flow can be accommodated with a milder water table gradient. Moreover, our simulations show that a water table within a homogeneous, isotropic cone only exists for a restricted range of recharge rates and permeabilities (Figure 3). Outside this range, the cone is either unsaturated or fully saturated. When permeabilities are anisotropic this effect can be much less pronounced (Figure 5b).

[44] Our simulations suggest that several conditions facilitate the ascent of a hydrothermal plume (defined for our purposes as a plume with elevated fluid temperatures containing some vapor): a sufficient heat source at depth to induce strong buoyancy forces; a deep flux of exsolved magmatic volatiles; a relatively weak topography-driven flow system; and the existence of a moderate-permeability ($k \geq 10^{-16}$ m^2) pathway between the deep high-temperature source and the shallow interior of the cone.

[45] The inferred limiting permeability of $k \geq 10^{-16}$ m^2 for the transition between advection- and conduction-dominated thermal regimes (Figure 9: simulation H1) is consistent with previous theoretical studies. High rates of heat exchange between magma and groundwater permit only a thin "conductive boundary layer" ($k \leq 10^{-17}$ m^2) between magma and actively circulating fluid [cf. *Lister*, 1974; *Lowell and Germanovich*, 1994].

[46] *Forster and Smith* [1989] demonstrated that an optimum permeability configuration for focused hydrothermal discharge is a subvertical, high-permeability conduit embedded in a moderate-permeability matrix. In the context of a volcanic edifice, the summit vent area (Figure 2) is an

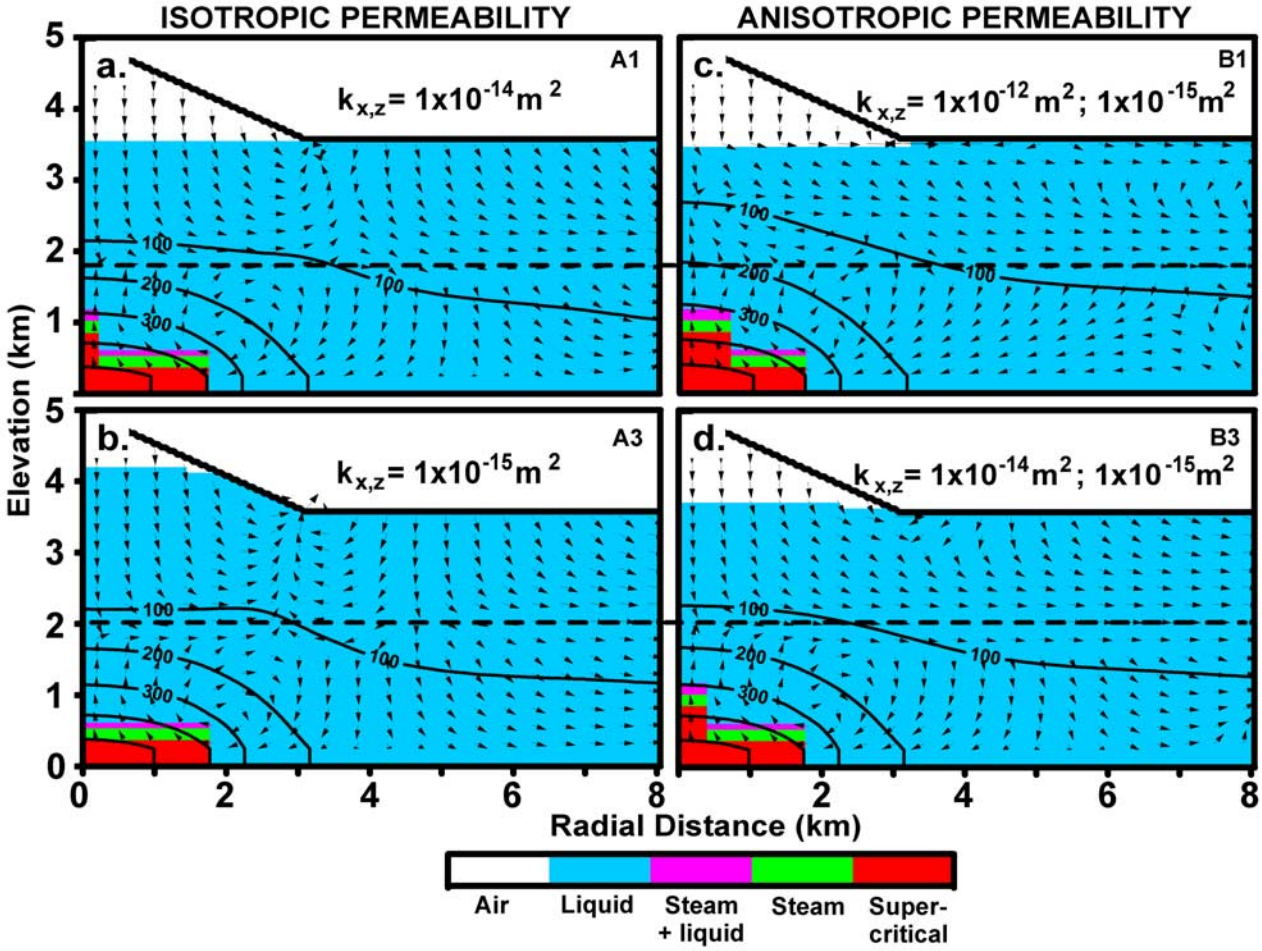

Figure 8. Patterns of fluid circulation, fluid-phase, and temperature for simulations (a) A1 and (b) A3 with varying isotropic permeability, and (c) B1 and (d) B3 with varying anisotropic permeability. Arrows indicate relative magnitude and direction of fluid flow; colors indicate the phase of the fluid. In all of these simulations the permeability of the basal unit was 1×10^{-17} m^2, basal heat input was 14 MW, and recharge into the cone was 0.1 m yr^{-1} (Table 3). The dashed horizontal line is the top of the basal unit.

obvious candidate location for the top of a conduit. However, a high-permeability conduit underlying the summit will not necessarily promote development of a hydrothermal plume because of the competing effect of topography-driven recharge (Figure 11).

7.2. Application to Stratovolcanoes in the Cascade Range

[47] The scarcity of deep drill holes on Cascade Range volcanoes limits our ability to directly infer the elevation of the water table or measure temperatures and pressures at depth. However, there are some data to guide our interpretation of the simulation results, including observations of fumaroles and thermal springs and a few borehole-temperature profiles, mainly from edifice flanks.

[48] There are important physiographic and hydrogeologic differences between the low-angle shield volcanoes and the steep stratovolcanoes in the Cascade Range (Figure 1). The shields have summit elevations of approximately 2500 m above mean sea level (msl), are usually ice free, and have little visible fumarolic activity. Newberry in Oregon and Medicine Lake in northern California, the best explored shield volcanoes in the Cascade Range, have shallow summit calderas partly occupied by lakes and road networks that have facilitated drilling of centrally located drill holes. Drilling has encountered temperatures of 265°C at a depth of 930 m in well USGS-N2 at Newberry Caldera [*Sammel et al.*, 1988] and 260°C at 2450 m in well 31-17 at Medicine Lake [*Lutz et al.*, 2000]. At Newberry, well bore temperature profiles indicate a complex pattern of high-temperature advective heat transport below about 300-m depth and seem to constrain the water table position to 0–300 m depth.

[49] Our simulations (Figure 2 and Table 3) focus on the steeper stratovolcanoes. These are believed to pose greater volcanic hazards than the shields because of their tendency toward more explosive eruptions and potential for slope failure and lahar generation. Stratovolcano summit elevations in the Cascade Range vary from ~3000 m (Mt. St. Helens after the 1980 eruption) to ~4400 m above msl (Mt. Rainier). Most stratovolcanoes have thick and extensive icecaps filling summit craters and flank valleys [*Driedger and Kennard*, 1986; *Kennard and Driedger*, 1986]. Of the Cascade Range

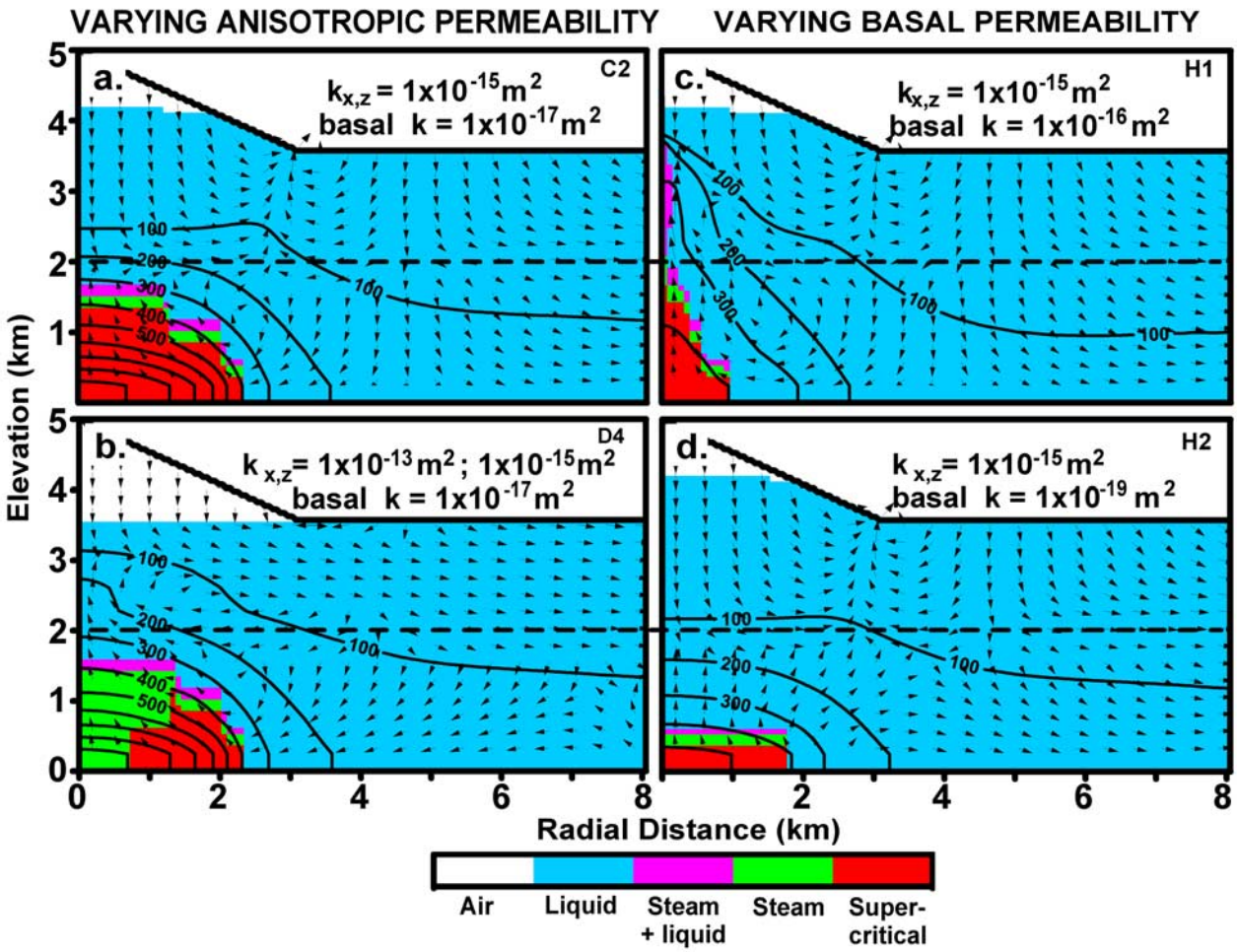

Figure 9. Patterns of fluid circulation, fluid-phase distribution, and temperature in simulations with relatively high heat input (28 MW) and (a) isotropic permeability and (b) anisotropic permeability and simulations with lower heat input (14 MW) and (c) relatively high basal permeability and (d) low basal permeability. Arrows indicate relative magnitude and direction of fluid flow; colors indicate the phase of the fluid. In all of these simulations recharge into the cone was 0.1 m yr^{-1}. The dashed horizontal line is the top of the basal unit.

stratovolcanoes, only the Crater Lake caldera, Oregon (former Mt. Mazama), has a large, exposed lake, although Mt. Rainier has a small lake under ice in one of its summit craters. Fumarolic activity at most of the stratovolcanoes is focused at the summit or within the summit crater with additional but generally less extensive activity on the flanks (e.g., Mt. Rainier, Mt. St. Helens, Mt. Hood, Mt. Shasta). At Mt. Baker, fumarolic activity occurs on the margins of the icecap at Sherman Crater, approximately 400 m below the summit [*Frank and Post*, 1976]. At some stratovolcanoes there is no apparent fumarolic activity (Mt. Jefferson, Mt. Adams). In the Cascade Range, lateral outflow of hydrothermal fluid from beneath many stratovolcanoes appears to feed high-chloride hot springs located up to tens of kilometers away [*Ingebritsen et al.*, 1989].

[50] Among the Cascade Range stratovolcanoes (Figure 1), Mt. Hood, Oregon, is relatively rich in drill hole information owing to geothermal reconnaissance in the 1970s and early 1980s. Even at Mt. Hood, however, all of the drill holes are at least a 5-km lateral distance from the summit, and the highest wellhead is nearly a 2-km vertical distance below the summit. Temperature profiles in drill holes indicate that heat flow increases toward the summit region, suggesting that the buoyancy forces advecting heat upward are relatively strong in comparison to the topography-driven flow system [*Nathenson and Tilling*, 1993]. The deep Pucci drill hole near Timberline Lodge was drilled to 1130-m depth from an elevation of 1628 m (1800 m below the summit). The standing water level in the Pucci well was 573 m below the land surface after completion of drilling in 1980 [*Robison et al.*, 1981]. Bottom hole temperature was 76°C. These data suggest that the water table under the volcano is relatively deep unless groundwater beneath the summit region is impounded by dikes, as originally proposed by O. E. Meinzer [*Stearns and Clark*, 1930] for Hawaiian volcanoes. An alternative explanation of the Pucci well water-level observations is that the water table is relatively shallow and that there is a large potential gradient for downward flow. For example, in simulation E2 the water table is located at the land surface, but the

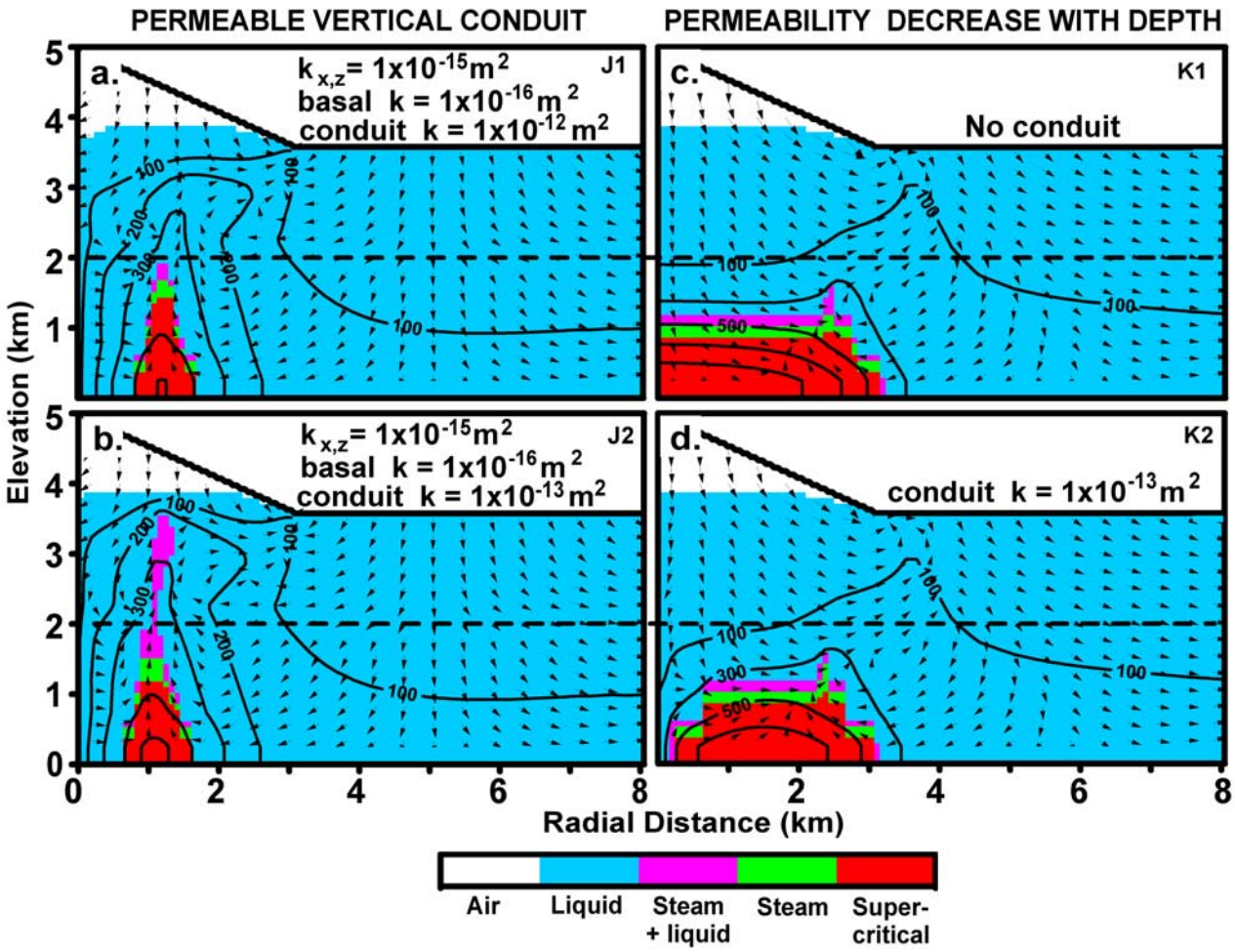

Figure 10. Patterns of fluid circulation, fluid-phase distribution, and temperature showing effects of a permeable vertical conduit in simulations (a) J1 and (b) J2 and effects of permeability decreasing with depth in simulations (c) K1 with a vertical permeable conduit and (d) K2 without a vertical conduit. Arrows indicate relative magnitude and direction of fluid flow; colors indicate the phase of the fluid. The dashed horizontal line is the top of the basal unit.

calculated pressure at 1130-m depth (Figure 12) would indicate a water table about 700 m below land surface.

[51] These sparse observations from Cascade Range stratovolcanoes best compare with simulations having a deep mass source, high heat input rates, $k \geq 1 \times 10^{-16}$ m^2 in the basal unit, anisotropic permeability in the upper unit, and a low precipitation-recharge rate (e.g., Figure 11: simulation L5). In such simulations the water table is near the base of the cone and a vapor phase and the 100°C isotherm are near the water table. This and similar simulations seem to capture the essential components of the system.

[52] The inferred low recharge rates are not consistent with watershed-scale water budget studies in Quaternary rocks of the Oregon Cascades that suggest precipitation recharge rates on the order of 1 m yr^{-1} [*Ingebritsen et al.*, 1992; *Manga*, 1997]. We speculate that near-summit recharge rates are significantly lower than those from the water budget studies because precipitation on a high edifice falls as snow and accumulates into thick glaciers that form seals, retarding percolation into the volcanic cone. Most glacial ice melts below the firn line, well below the summit of the volcano. This could tend to reduce subsummit water table elevations and weaken the topography-driven flow systems, enhancing the probability of significant hydrothermal upflow.

[53] The inference of a permeable conduit existing from the land surface to near-magma depths contrasts with results of laboratory experiments in crystalline rocks and theoretical studies, which have demonstrated that in hydrothermal systems secondary mineral precipitation and thermomechanical forces can decrease permeabilities from 1×10^{-16} m^2 to less than 1×10^{-20} m^2 in as little as several days [*Vaughan et al.*, 1986; *Moore et al.*, 1994; *Martin and Lowell*, 1997]. Perhaps frequent seismicity is required to maintain sufficient effective permeability for hydrothermal upflow over time. Several sets of observations suggest a causal relationship between deep hydrothermal circulation and low-level seismicity [*Saar and Manga*, 2003]. At Mt. Rainier, Mt. St. Helens, and Mt. Hood (Figure 1), several high-frequency volcano-tectonic earthquakes occur each month at depths of 3 km or greater beneath the summit [*Moran*, 1994;

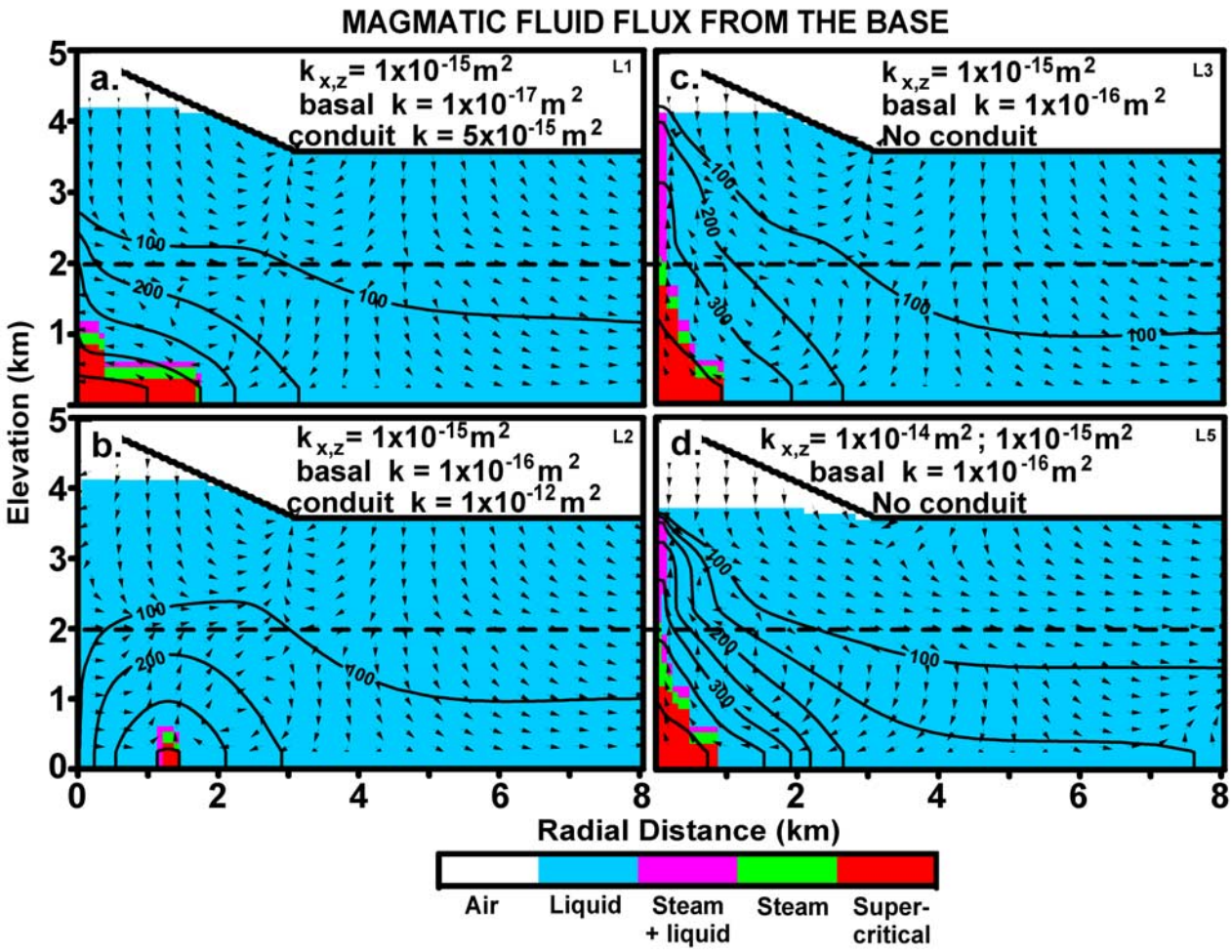

Figure 11. Patterns of fluid circulation and fluid-phase distribution and temperature for selected simulations with magmatic fluid input at depth with a high-permeability conduit (a) L1 and (b) L2 and without a high-permeability conduit (c) L3 and (d) L5. Arrows indicate relative magnitude and direction of fluid flow; colors indicate the phase of the fluid. The dashed horizontal line is the top of the basal unit.

Moran et al., 2000; *Saar and Manga*, 2003]. At Mt. Hood, seismicity is distributed southward from the summit region [*Weaver et al.*, 1990], approaching the vicinity of the only hydrothermal manifestation on the flanks, Swim Warm Springs.

[54] The Lassen volcanic system in northern California (Figure 1) illustrates that advection (and hence $k \geq 10^{-16}$ m^2) must be the dominant heat transport mechanism between the magmatic envelope and the shallow subsurface. In Lassen, the measured heat discharge from hydrothermal features totals over 100 MW [*Sorey and Colvard*, 1994]. Such rates of heat discharge have likely persisted for at least 80 years [*Ingebritsen et al.*, 2001]. The heat is probably derived from a small silicic magma body emplaced at a depth of at least several kilometers, with a heat transfer area of no more than a few square kilometers. If we take the heat transfer area to be <5 km^2, the average conductive heat flux over that area must be >20 W m^{-2}. If we then assume a reasonable thermal conductivity of 2 W m^{-2} K^{-1} and a temperature difference of 500°C between the magma body (800°C) and circulating groundwater (300°C), then the conductive ($k \leq 1 \times 10^{-17}$ m^2) length between the magma and the actively circulating hydrothermal system must be <50 m.

[55] The presence or absence of a vapor-phase or boiling plume within a volcano is relevant to the level of volcanic hazard. Localized or pervasive hydrothermal alteration affects the structural integrity and mechanical strength of the edifice [*Lopez and Williams*, 1993; *Reid et al.*, 2001]. High-temperature, argillic "acid-sulfate" alteration associated with a vapor phase or boiling fluid is generally weakening, with the mechanical strength of the altered material less than that of the original rock. It is believed that some Andean stratovolcanoes are pervasively altered by hydrothermal plume activity and therefore weak (W. Hildreth, U.S. Geological Survey, oral communication, 2003). An analogy that has been suggested is a chocolate-dipped ice cream cone, a rigid carapace overlying soft, weakened material. However, most Cascade Range stratovolcanoes seem to be much less pervasively altered and presumably stronger (T. Sisson, U.S. Geological Survey, written communication, 2003), implying that zones of argillic alteration within the edifice are confined and narrow. For example, airborne electromagnetic and mag-

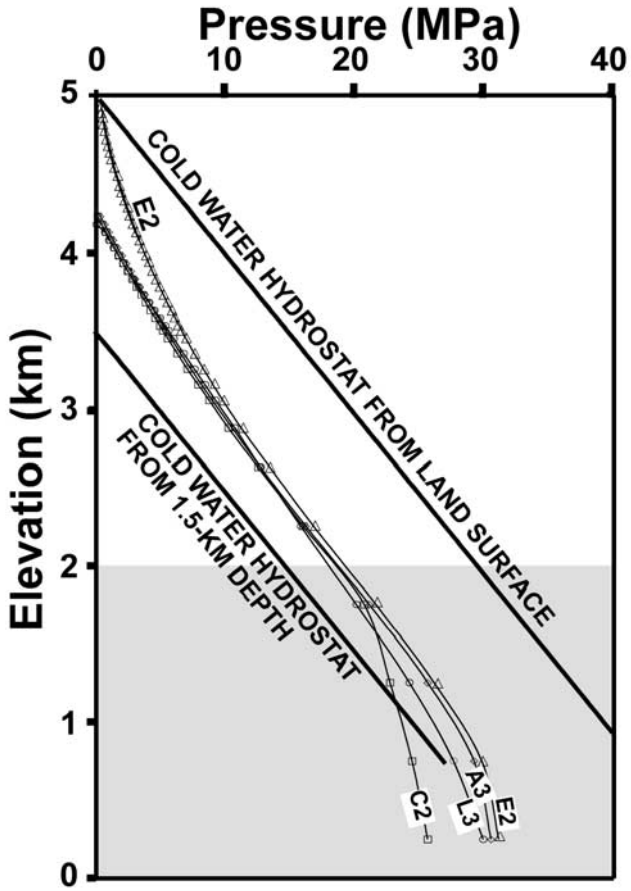

Figure 12. Calculated pressure profiles near the axis of the domain (r = 25 m) for selected simulations. Gray shading is basal unit.

netic data from Mt. Rainier show that hydrothermally altered rock (mostly buried) occurs mainly within the upper west flank of the volcano, where it is associated with a zone of open fractures and radial dikes emplaced during episodes of heightened magmatic activity. Much of the altered material under the summit was removed by the Osceola Mudflow 5600 years ago [*Vallance and Scott*, 1997]. Currently, negligible amounts of altered rock lie in the volcano's core, where stronger rocks would impede collapse retrogression and limit the volumes and inundation areas of debris flows [*Finn et al.*, 2001; *Reid et al.*, 2001].

[56] The presence or absence of a hydrothermal plume within a volcano is also relevant to the potential for geothermal resources and mineralization. Our simulations suggest that only under a narrow range of conditions (e.g., Figure 8, simulation H1; Figure 11, simulation L3) will a high water table (thus sufficient water for production) and a significant hydrothermal plume develop within the edifice. Therefore expensive drilling for geothermal exploration on upper flanks of Cascade Range stratovolcanoes is unlikely to be productive. The simulation results also suggest that ore minerals associated with argillic acid-sulfate alteration, usually related to a boiling fluid, may often be restricted to deeper parts of the edifice and/or to fracture zones near the central vent of the volcano.

7.3. Implications of a Deep Water Table

[57] Both our simulation results and the sparse field observations from Mt. Hood suggest that water tables within Cascade Range stratovolcanoes may be relatively deep, as seems to be the case for many Hawaiian volcanoes, despite high recharge rates [e.g., *Stearns and Clark*, 1930; *Stearns and MacDonald*, 1946]. A deep water table has implications for several classes of volcanic hazards. For instance, above the water table there cannot be significantly elevated fluid pressures to enhance the potential for slope failure (although there could be local zones of perched water). Phreatic eruptions from volcanoes with deep water tables are not likely to occur in response to groundwater flow toward the conduit [*Mastin*, 1997] but might be triggered instead by shallow intrusion and localized recharge by melted snow and ice. Water to generate lahars would be unlikely to come from the saturated zone but might be supplied by snow and ice and shallow groundwater "perched" on low-permeability altered zones.

[58] A cone that is fully saturated by cold groundwater under near-hydrostatic conditions will tend to suppress hydrothermal upflow. Thus the presence of hydrothermal discharge or pervasive alteration high on the edifice

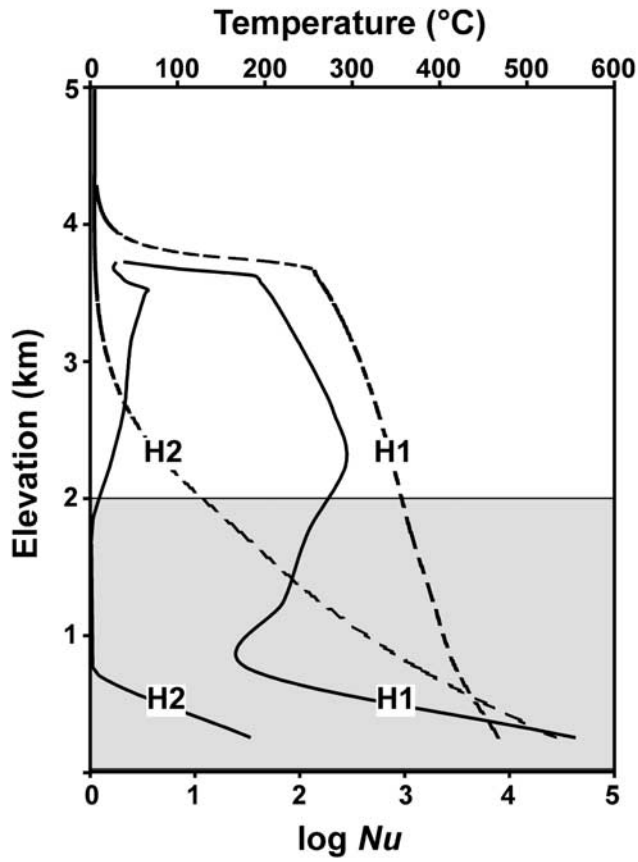

Figure 13. Calculated temperature (dashed) and log *Nu* (solid) profiles for simulations H1 and H2 (Figures 9c and 9d and Table 3) at a radial distance of 25 m from the axis of the domain. Gray shading is basal unit.

supports the supposition that topography-driven downflow is somehow restricted. The necessary restriction may be related to permeability heterogeneity and/or the availability of precipitation recharge. As the edifice evolves over geologic time, there may be a positive feedback between hydrothermal alteration and water table elevation as alteration tends to decrease the permeability of the rock as well as its mechanical strength [*Hurwitz et al.*, 2002].

7.4. Future Work

[59] The simulations we report here lay a foundation for future field and theoretical investigations. Deep drilling high on stratovolcanoes in the Cascade Range is logistically challenging, expensive, and unlikely to occur in the near future. Thus observational investigations must rely on inference. We suggest that high-resolution airborne measurements of electrical resistivity, magnetic susceptibility, and visible/infrared imaging spectrometry (AVIRIS), that were applied successfully at Mt. Rainier [*Crowley and Zimbelman*, 1997; *Finn et al.*, 2001] may help to better define the distribution of hydrothermal fluids and/or alteration within volcanic edifices. Long-term, high-frequency measurements of steam and gas discharge and correlation of these data with seismic and stress measurements may allow inferences regarding the dynamics of these systems, in particular the relationship between hydrothermal circulation, deformation, and seismicity. Finally, field observation and mapping of groundwater discharge under late summer conditions may help to define water table elevations.

[60] In this paper we have focused on quasi steady state numerical simulations in order to evaluate the sensitivity of water table elevation and hydrothermal circulation to controlling parameters and to facilitate comparison with steady state results reported by previous investigators. The resulting suite of quasi-steady solutions (Table 3), obtained through long-term transient simulations, also prepares the way for meaningful simulation of shorter-term transient effects. It defines feasible sets of initial conditions for simulation of transient processes such as injection of magmatic heat and fluids, changes in the rates and distribution of precipitation recharge, or system modification due to geothermal development.

8. Summary and Conclusions

[61] We have modified the HYDROTHERM numerical simulator to include several additional types of boundary conditions, which allowed simulations that represent continental volcano-hydrothermal systems. We evaluated the sensitivity of water table elevation and hydrothermal circulation to a wide range of recharge rates, heat input rates, and hydraulic parameters. Simulation results were compared to observations from the Quaternary stratovolcanoes along the Cascade Range in the western United States to obtain information about hydrothermal processes.

[62] The permeability structure of the volcanic edifice and underlying material is the dominant control on water table configuration and the distribution of pressures, temperatures, and fluid phases at depth. Active hydrothermal circulation within the edifice requires a pathway with a time-averaged permeability of at least $k \geq 10^{-16}$ m^2 to exist between a high-temperature source and the interior of the cone. Such a permeability may be maintained by frequent seismicity. In our simulations with a low-permeability basal unit ($\leq 1 \times 10^{-17}$), heat transport at depth is dominated by conduction and temperatures at shallow depths remain well below the boiling curve.

[63] Several conditions facilitate the ascent of a hydrothermal plume into a volcanic edifice: a sufficient source of heat and magmatic volatiles at depth, strong buoyancy forces, and a relatively weak topography-driven flow system. Deep recharge of cold groundwater may be restricted by low edifice permeability and/or the lack of precipitation. Extensive ice cover on most Cascade Range stratovolcanoes may restrict recharge beneath the summits.

[64] Both our simulation results and the sparse field observations allow the possibility that the water table beneath Cascade Range stratovolcanoes is relatively deep, implying (1) a weak topography-driven flow system, enhancing the probability of hydrothermal upflow, (2) an absence of significantly elevated fluid pressures in the uppermost part of the cone, (3) that phreatic eruptions from such volcanoes are not likely to occur in response to groundwater flow toward the conduit, and (4) that large volumes of water necessary to generate lahars would be unlikely to come from the saturated zone but might be supplied by snow, ice, and shallow "perched" groundwater.

[65] **Acknowledgments.** We thank Grant Garven, Larry Mastin, Martin Saar, Tom Sisson, and Claire Tiedeman for very helpful comments and constructive reviews.

References

Black, G. L., Newberry hydrology, *Oreg. Dep. Geol. Miner. Ind. Open File Rep. O-83-3*, pp. 29–36, 1983.

Blackwell, D. D., R. G. Bowen, D. A. Hull, J. Riccio, and J. L. Steele, Heat flow, arc volcanism, and subduction in northern Oregon, *J. Geophys. Res.*, *87*, 8735–8754, 1982.

Brace, W. F., Permeability of crystalline and argillaceous rocks, *Int. J. Rock Mech. Min. Sci. Geomech. Abstr.*, *17*, 241–251, 1980.

Brace, W. F., Permeability of crystalline rocks: New in situ measurements, *J. Geophys. Res.*, *89*, 4327–4330, 1984.

Buettner, R., B. Zimanowski, J. Blumm, and L. Hagemann, Thermal conductivity of a volcanic rock material (olivine-melilitite) in the temperature range between 288 and 1470 K, *J. Volcanol. Geotherm. Res.*, *80*, 293–302, 1998.

Cathles, L. M., An analysis of the cooling of intrusives by ground-water convection which includes boiling, *Econ. Geol.*, *72*, 804–826, 1977.

Clauser, C., Opacity: The concept of radiative thermal conductivity, in *Handbook of Terrestrial Heat-Flow Density Determination*, edited by R. Haenel, pp. 143–165, Kluwer Acad., Norwell, Mass., 1988.

Crowley, J. K., and D. R. Zimbelman, Mapping hydrothermally altered rocks on Mount Rainier, Washington, with Airborne Visible/Infrared Imaging Spectrometer (AVIRIS) data, *Geology*, *25*, 559–562, 1997.

Driedger, C. L., and P. M. Kennard, Ice volumes on Cascade volcanoes: Mount Rainier, Mount Hood, Three Sisters, and Mount Shasta, *U.S. Geol. Surv. Prof. Pap., 1365*, 28, 1986.

Faust, C. R., and J. W. Mercer, Geothermal reservoir simulation, 1, Mathematical models for liquid- and vapor-dominated hydrothermal systems, *Water Resour. Res.*, *15*, 23–30, 1979.

Finn, C. A., T. W. Sisson, and M. Deszcz-Pan, Aerogeophysical measurements of collapse-prone hydrothermally altered zones at Mount Rainier Volcano, *Nature*, *409*, 600–603, 2001.

Forster, C. B., and L. Smith, Groundwater flow systems in mountainous terrain, 1, Numerical modeling technique, *Water Resour. Res.*, *24*, 999–1010, 1988a.

Forster, C. B., and L. Smith, Groundwater flow systems in mountainous terrain: 2. Controlling factors, *Water Resour. Res.*, *24*, 1011–1023, 1988b.

Forster, C. B., and L. Smith, The influence of groundwater flow on thermal regimes in mountainous terrain: A model study, *J. Geophys. Res.*, *94*, 9439–9451, 1989.

Frank, D. G., Surficial extent and conceptual model of hydrothermal system at Mount Rainier, Washington, *J. Volcanol. Geotherm. Res.*, *65*, 51–80, 1995.

Frank, D. G., and A. S. Post, Hydrothermal activity at Mount Baker, Washington, *U.S. Geol. Surv. Prof. Pap., 1000*, 170–171, 1976.

Friedman, J. D., D. L. Williams, and D. Frank, Structural and heat flow implications of infrared anomalies at Mt. Hood, Oregon, 1972–1977, *J. Geophys. Res.*, *87*, 2793–2803, 1982.

Hanson, R. B., Hydrodynamics of magmatic and meteoric fluids in the vicinity of granitic intrusions, *Spec. Pap. Geol. Soc. Am.*, *315*, 251–259, 1996.

Hasabe, K., N. Fujii, and S. Uyeda, Thermal processes under island arcs, *Tectonophysics*, *10*, 335–355, 1970.

Hayba, D. O., and S. E. Ingebritsen, The computer model HYDROTHERM, a three-dimensional finite-difference model to simulate ground-water flow and heat transport in the temperature range of 0 to 1,200 degrees Celsius, *U.S. Geol. Surv. Water Res. Invest. Rep. 94-4045*, 85 pp., 1994.

Hayba, D. O., and S. E. Ingebritsen, Multiphase groundwater flow near cooling plutons, *J. Geophys. Res.*, *102*, 12,235–12,252, 1997.

Hurwitz, S., S. E. Ingebritsen, and M. L. Sorey, Episodic thermal perturbations associated with groundwater flow: An example from Kilauea Volcano, Hawaii, *J. Geophys. Res.*, *107*(B11), 2297, doi:10.1029/2001JB001654, 2002.

Ingebritsen, S. E., and W. E. Sanford, *Groundwater in Geologic Processes*, Cambridge Univ. Press, New York, 1998.

Ingebritsen, S. E., D. R. Sherrod, and R. H. Mariner, Heat flow and hydrothermal circulation in the Cascade Range, north-central Oregon, *Science*, *243*, 1458–1462, 1989.

Ingebritsen, S. E., D. R. Sherrod, and R. H. Mariner, Rates and patterns of groundwater flow in the Cascade Range volcanic arc, and the effect on subsurface temperatures, *J. Geophys. Res.*, *97*, 4599–4627, 1992.

Ingebritsen, S. E., R. H. Mariner, and D. R. Sherrod, Hydrothermal systems of the Cascade Range, north-central Oregon, *U.S. Geol. Surv. Prof. Pap., 1044-L*, 86, 2 plates, 1994.

Ingebritsen, S. E., D. L. Galloway, E. M. Colvard, M. L. Sorey, and R. H. Mariner, Time-variation of hydrothermal discharge at selected sites in the western United States: Implications for monitoring, *J. Volcanol. Geotherm. Res.*, *111*, 1–23, 2001.

Iverson, R. M., and M. E. Reid, Gravity-driven groundwater flow and slope failure potential, 1, Elastic effective-stress model, *Water Resour. Res.*, *28*, 925–938, 1992.

Jamieson, G. R., and R. A. Freeze, Determining hydraulic conductivity distributions in a mountainous area using mathematical modeling, *Ground Water*, *21*, 168–177, 1983.

Keller, G. V., L. T. Grose, J. C. Murray, and C. K. Skokan, Results of an experimental drill hole at the summit of Kilauea Volcano, Hawaii, *J. Volcanol. Geotherm. Res.*, *5*, 345–385, 1979.

Kennard, P. M., and C. L. Driedger, Estimated ice volumes on Cascade volcanoes: Mounts Baker, Glacier, Adams, and Jefferson (abstract), *Geol. Soc. Am. Abstr. Programs*, *18*, 124, 1986.

Lister, C. R. B., On the penetration of water into hot rock, *Geophys. J. R. Astron. Soc.*, *39*, 465–509, 1974.

Lopez, D. L., and S. N. Williams, Catastrophic volcanic collapse: Relation to hydrothermal processes, *Science*, *260*, 1794–1796, 1993.

Lowell, R. P., and L. N. Germanovich, On the temporal evolution of high-temperature hydrothermal systems at ocean ridge crests, *J. Geophys. Res.*, *99*, 565–575, 1994.

Lutz, S. J., J. B. Hulen, and A. Schriener, Alteration, geothermometry, and granitoid in Well 37-17, Medicine Lake Volcano geothermal system, California, paper presented at 25th Workshop on Geothermal Reservoir Engineering, Stanford Univ., Stanford, Calif., 2000.

Manga, M., Hydrology of spring-dominated streams in the Oregon Cascades, *Water Resour. Res.*, *32*, 2435–2439, 1996.

Manga, M., A model for discharge in spring-dominated streams and implications for the transmissivity and recharge of Quaternary volcanics in the Oregon Cascades, *Water Resour. Res.*, *33*, 1813–1822, 1997.

Manning, C. E., and S. E. Ingebritsen, Permeability of the continental crust: Implications of geothermal data and metamorphic systems, *Rev. Geophys.*, *37*, 127–150, 1999.

Manning, C. E., S. E. Ingebritsen, and D. K. Bird, Missing mineral zones in contact metamorphosed basalts, *Am. J. Sci.*, *293*, 894–938, 1993.

Mariner, R. H., T. S. Presser, W. C. Evans, and M. K. W. Pringle, Discharge rates of fluid and heat by thermal springs of the Cascade Range, Washington, Oregon, and northern California, *J. Geophys. Res.*, *95*, 19,517–19,532, 1990.

Martin, J. T., and R. P. Lowell, On thermoelasticity and silica precipitation in hydrothermal systems: Numerical modeling of laboratory experiments, *J. Geophys. Res.*, *102*, 12,095–12,107, 1997.

Mastin, L. G., Evidence for water influx from a caldera lake during the explosive eruption of 1790, Kilauea Volcano, Hawaii, *J. Geophys. Res.*, *102*, 20,093–20,109, 1997.

Moore, D. E., D. A. Lockner, and J. D. Byerlee, Reduction of permeability in granite at elevated temperatures, *Science*, *265*, 1558–1561, 1994.

Moran, S. C., Seismicity at Mount St. Helens, 1987–1992: Evidence for repressurization of an active magmatic system, *J. Geophys. Res.*, *99*, 4341–4354, 1994.

Moran, S. C., D. R. Zimbelman, and S. D. Malone, A model for the magmatic-hydrothermal system at Mount Rainier, Washington, from seismic and geochemical observations, *Bull. Volcanol.*, *61*, 425–436, 2000.

Nathenson, M., and R. I. Tilling, Conductive heat transfer from an isothermal magma chamber and its application to the measured heat flow distribution from Mount Hood, Oregon, *Trans. Geotherm. Resour. Counc.*, *17*, 141–148, 1993.

Norton, D., and J. E. Knight, Transport phenomena in hydrothermal systems: Cooling plutons, *Am. J. Sci.*, *277*, 937–981, 1977.

Nur, A., and J. Walder, Hydraulic pulses in the Earth's crust, in *Fault Mechanics and Transport Properties of Rocks*: *A Festschrift in Honor of W. F. Brace*, edited by B. Evans and T. F. Wong, pp. 461–474, Academic, San Diego, Calif., 1992.

Reid, M. E., and R. M. Iverson, Gravity-driven groundwater flow and slope failure potential: 2. Effects of slope morphology, material properties, and hydraulic heterogeneity, *Water Resour. Res.*, *28*, 939–950, 1992.

Reid, M. E., T. W. Sisson, and D. L. Brien, Volcano collapse promoted by hydrothermal alteration and edifice shape, Mount Rainier, Washington, *Geology*, *29*, 779–782, 2001.

Robison, J. H., L. S. Forcella, and M. W. Gannett, Data from geothermal test wells near Mount Hood, Oregon, *U.S. Geol. Surv. Open File Rep. OF 81-1002*, 26 pp., 1981.

Saar, M. O., and M. Manga, Seismicity induced by seasonal groundwater recharge at Mt. Hood, Oregon, *Earth Planet. Sci. Lett.*, *214*, 605–618, 2003.

Sammel, E. A., S. E. Ingebritsen, and R. H. Mariner, The hydrothermal system at Newberry Volcano, Oregon, *J. Geophys. Res.*, *93*, 10,149–10,162, 1988.

Smith, L., and D. S. Chapman, On the thermal effects of groundwater flow, *J. Geophys. Res.*, *88*, 593–608, 1983.

Sorey, M. L., and E. M. Colvard, Measurements of heat and mass flow from thermal areas in Lassen Volcanic National Park, California, *U.S. Geol. Surv. Water Res. Invest. Rep., 94-4180-A*, 35, 1994.

Souza, W. R., and C. I. Voss, Analysis of an anisotropic coastal aquifer system using variable-density flow and transport simulation, *J. Hydrol.*, *92*, 17–41, 1987.

Stearns, H. T., and W. O. Clark, Geology and water resources of the Kau District, Hawaii, *U.S. Geol. Surv. Water Supply Pap., 616*, 194, 1930.

Stearns, H. T., and G. A. MacDonald, Geology and ground-water resources on the island of Hawaii, *Hawaii Div. Hydrogr. Bull.*, *9*, 362 pp., 1946.

Takasaki, K. J., Ground water in Kilauea and adjacent areas of Mauna Loa Volcano, Hawaii, *U.S. Geol. Surv. Open File Rep., 93-82*, 28, 1993.

Terzaghi, K., *Theoretical Soil Mechanics*, 528 pp., John Wiley, Hoboken, N. J., 1943.

Vallance, J. W., and K. M. Scott, The Osceola Mudflow from Mount Rainier: Sedimentology and hazard implications of a huge clay-rich debris flow, *Geol. Soc. Am. Bull.*, *109*, 143–163, 1997.

Varekamp, J. C., and G. L. Rowe (Eds.), Crater Lakes, *J. Volcanol. Geotherm. Res.*, *97*, 508 pp., 2000.

Vaughan, P. J., D. E. Moore, C. A. Morrow, and J. D. Byerlee, Role of cracks in progressive permeability reduction during flow of heated aqueous fluids through granite, *J. Geophys. Res.*, *91*, 7517–7530, 1986.

Weaver, C. S., R. D. Norris, and C. Trisler-Jonientz, Results of seismological monitoring in the Cascades Range 1962–1989: Earthquakes, eruptions, avalanches, and other curiosities, *Geosci. Can.*, *17*, 158–162, 1990.

Winograd, I. J., Hydrogeology of ash-flow tuff: A preliminary statement, *Water Resour. Res.*, *7*, 994–1006, 1971.

S. Hurwitz, S. E. Ingebritsen, and M. E. Reid, U.S. Geological Survey, 345 Middlefield Road, MS 439, Menlo Park, CA 94025, USA. (shaulh@usgs.gov)

K. L. Kipp, U.S. Geological Survey, Denver Federal Center, MS 413, Box 25406, Denver, CO 80225, USA.